

Review

Seismic Assessment of Large-Span Spatial Structures Considering Soil–Structure Interaction (SSI): A State-of-the-Art Review

Puyu Zhan, Suduo Xue, Xiongyan Li *, Guojun Sun and Ruisheng Ma

Faculty of Architecture, Civil and Transportation Engineering, Beijing University of Technology, Beijing 100124, China

* Correspondence: xylee@bjut.edu.cn

Abstract: Soil–structure interaction (SSI), which characterizes the dynamic interaction between a structure and its surrounding soil, is of great significance to the seismic assessment of structures. Past research endeavors have undertaken analytical, numerical, and experimental studies to gain a thorough understanding of the influences of SSI on the seismic responses of a wide array of structures, including but not limited to nuclear power plants, frame structures, bridges, and spatial structures. Thereinto, large-span spatial structures generally have much more complex configurations, and the influences of SSI may be more pronounced. To this end, this paper aims to provide a state-of-the-art review of the SSI in the seismic assessment of large-span spatial structures. It begins with the modelling of soil medium, followed by the research progress of SSI in terms of numerical simulations and experiments. Subsequently, the focus shifts towards high-lighting advancements in understanding the seismic responses of large-span spatial structures considering SSI. Finally, some discussions are made on the unresolved problems and the possible topics for future studies.

Keywords: soil–structure interaction; state-of-the-art review; large-span spatial structure; seismic assessment



Citation: Zhan, P.; Xue, S.; Li, X.; Sun, G.; Ma, R. Seismic Assessment of Large-Span Spatial Structures Considering Soil–Structure Interaction (SSI): A State-of-the-Art Review. *Buildings* **2024**, *14*, 1174. <https://doi.org/10.3390/buildings14041174>

Academic Editor: Fabrizio Gara

Received: 27 February 2024

Revised: 9 April 2024

Accepted: 17 April 2024

Published: 21 April 2024



Copyright: © 2024 by the authors. Licensee MDPI, Basel, Switzerland. This article is an open access article distributed under the terms and conditions of the Creative Commons Attribution (CC BY) license (<https://creativecommons.org/licenses/by/4.0/>).

1. Introduction

Soil–structure interaction (SSI) has become one of the most concerning research topics in the field of earthquake engineering, especially with the development of complicated structures, i.e., high-rise buildings and large-span spatial structures. The concept of SSI can be traced back to 1936 [1], with the initial emphasis laid on the interaction between the soil and underground structures. In the subsequent decades, extensive investigations delved into SSI, expanding its scope to encompass structures both above and below the ground. Generally speaking, SSI can be categorized into two types, namely the kinematic interaction and inertial interaction. Specifically, the kinematic interaction involves the impact of vibrational feedback from the superstructure on the amplitude and spectral composition of foundation motion. This reduces the acceleration amplitude of the foundation below that of the neighboring free field, simultaneously enhancing the components around the fundamental frequencies of structures. Additionally, the flexibility of the soil foundation contributes to the frequencies and modes of vibration of the superstructure, with softer foundations generally prolonging the structural period. The inertial interaction encompasses the dissipation of energy resulting from the vibrations of the superstructure subjected to inertial forces, attributed to phenomena such as reflection and diffraction [2,3]. A technical report published by the Federal Emergency Management Agency (FEMA) of the U.S. Department of Homeland Security (DHS) [4] distilled both interactions into three primary effects: the flexible foundation effect, kinematic effect, and foundation damping effect.

Structure–soil–structure interaction (SSSI), a specialized case of SSI, has played a pivotal role in assessing the impact of reactor vibration waves on neighboring nuclear

power plant (NPP) complexes through the soil medium for over half a century. It is considered a fundamental dynamic characteristic of NPP reactors [5]. Concurrently, with the ongoing trend of urbanization giving rise to denser complexes to accommodate a growing population, the SSSI effect is gradually becoming integral to the design of large-scale civil structures. This integration is commonly referred to as site–city interaction (SCI). Additionally, the SSSI effect between underground structures and nearby above-ground structures is gaining attention in the ongoing development and utilization of urban underground spaces. This is particularly significant, exemplified by the amplifying effect on low-rise buildings near high-rise structures [6].

When considering the effects of soil and foundations on the seismic response of superstructures, the primary factors can be broadly categorized into four main groups: structural type, foundation form, site effects, and seismic excitation. To date, frame structures and bridge engineering are focal points in SSI research. In both numerical and experimental investigations of SSI, more than half of the addressed superstructures involve multi-layer frame structures and adjacent steel or concrete structures [7]. Sections 3 and 4 will go into more detail on these structures. The dynamic characteristics of the majority of bridge structures are significantly impacted by SSI/SSSI [8,9], as has been demonstrated in subsequent earthquakes [10]; therefore, it has been currently integrated into the bridge design guidelines of many nations and is being used to guide the engineering practice of numerous bridges [11], whereas fewer studies are referring to the SSI effect of large-span spatial structures [12–17]. Large-span spatial structures include shell structures, grid structures, cable-suspended structures, etc., whose vibration subjected to seismic loads is three-dimensional. Since the dynamic characteristics of large-span spatial structures are different from bridges or high-rise buildings, the relatively mature SSI-effect research results for the latter two cannot be directly applied to the design calculation of the former. Meanwhile, when the vertical projection surface of the structure is large or too long and the foundation form adopts an independent pile foundation, it may produce a foundation–soil–foundation interaction (FSFI) effect; therefore, it is necessary to conduct more in-depth studies to investigate the SSI effect of large-span spatial structures. The foundation is a load-bearing structure that connects the superstructure and soil. According to Chinese regulations [18], the foundations are classified as pile foundations, extended foundations, and raft foundations, and the influence of the coefficient of which varies for superstructures according to the SSI/SSSI effect as well [19,20]. One of the key elements altering structural seismic damage is the site effect [21]. Based on the investigation of the 1985 Michoacan, Mexico, earthquake, local site effects were accountable for the uncommonly high ground accelerations [22]. This was because Michoacan is situated on top of a basin with a deep layer of soft soil that causes certain frequencies of ground movements to be dramatically amplified on the surface [23], while the basin has a focusing effect on the propagation of seismic waves within the soil layer [24]. It has been noted that topographic features (such as basins, canyons [25,26], summits, etc.) and soil properties make up the majority of the site conditions. Most of the research on SSI/SSSI is predicated on the assumption of being plain; nevertheless, there are projects constructed on slopes in practice. Moreover, it has been noticed that structures on adjacent slopes are more vulnerable [27], which cannot be disregarded when the ratio of the net distance of the structural foundation from the slope peak to its height is less than 5 [27]. Apart from the slope–foundation–structure system [28,29], the SSSI effects of structures on [30] and near [31] slopes have also been explored, which are known as the topography–soil–structure interaction (TSSI) and topography–structure–soil–structure interaction (TSSSI). Soil properties are a decisive component of SSI, and the numerical modelling techniques for soil determine the ability to realistically predict the propagation of seismic waves [32,33], as will be specified in the next section.

Seismic excitation refers to the entire process of seismic wave propagation from the source upward to the foundation–structure/surface, where the soil traversed by the seismic wave is defined as the free field [34] which is proposed to calculate the vibration response of soil under shear wave excitation, on the premise of assuming that the soil layer is

horizontal and homogeneous along the horizontal plane. A function consisting of source effects, travel path effects, and local site effects expresses the free-field ground motion under seismic excitation. Source distance and source count are two categories for the source effect. Based on the distance from the epicentre, earthquakes can be categorized into far-field and near-field ground motion [35], corresponding earthquake groupings are included in the code for the seismic design of buildings [36]. Compared with the former, the latter typically has a longer period and higher amplitude [37], which aggravates the seismic effect of non-flat sites [38]. Meanwhile, the continuous vibration caused by multiple sources probably exacerbates the damage to surface structures [22]. The travel path effect consists of the incoherence effect, wave-passage effect and the attenuation effect [39]. The correlation of seismic waves across separate spaces and times during their propagation is what describes the coherence of seismic waves. When seismic waves travel through uneven soil, the superposition of waves in different spaces on account of reflection and refraction results in the formation of different phases and elimination of interference, which is the incoherence effect. When the structure is so enormous that the time difference between the seismic wave arriving at each point is insurmountable, an occurrence known as the wave-passage effect arises. The attenuation effect is the steady decline in amplitude created by the geometric diffusion of seismic waves in the site's space. Throughout the process of site propagation, seismic waves may shift in space also to time, especially for some large spatial formations [40,41]. The spatial characteristics of ground motion comprise the aforementioned three effects as well as local site effects.

This paper provides a state-of-the-art review of the classification of SSI and the current state of theoretical research. Additionally, it summarizes previous numerical and experimental studies, along with existing research results. The work also delves into the significance of accounting for SSI effects in the seismic design of large-span spatial structures, discussing potential avenues for further studies. It is important to note that while this paper briefly reviews the SSI effect and does not delve into the influence of SSI on structural vibration control, it underscores the importance of considering the SSI effect in the actual design of seismic mitigation or isolation.

2. Modeling of Soil Medium

To simulate soil on SSI, two types of solutions are widely utilized [42], including the direct approach, which is typically realized through the finite element method (FEM) and the substructure approach. The concept of the foundation impedance function is introduced by the boundary substructure approach, whose applications to various sites and foundations are discussed in detail in the technical report (NIST/GCR 12-917-2) [43]. Springs and dampers are used to mimic the stiffness and damping at the soil–foundation interface. The Winkler model and its variants are typically employed in conjunction with the elastic half-space model for deep foundation systems, while the latter model is typically used for shallow foundation systems.

2.1. Winkler Model

Understanding the mechanical properties of the soil surrounding underground construction or foundation is crucial in the exploration of SSI. In the case of pile foundations, a widely used method to simplify soil behavior is the Winkler foundation beam model, which essentially comprises a system of closely spaced discrete spring and dampers that serves as a substitute for the dynamic impedance imposed by the soil on the pile body [44]. The Winkler model, being a one-parameter model, has limitations as it inaccurately assumes that discrete springs cannot replicate continuous soil deformation. In contrast to real-world scenarios, the model predicts only vertical displacement at a point of application. To overcome this limitation, various enhancements have been introduced, incorporating additional parameters such as tension, shear force, and bending moment. This has led to the development of two-parameter and three-parameter Winkler models, including notable

variants like the Filonenko-Borodich model, Hetenyi model, Pasternak model, and Kerr model [45].

In extending the elastic foundation formulas, Jemielita [46] synthesized monomial multiparameter formulas into differential formulas for multiple parameters and introduced the n Shear layer-Bending layer-Spring layer (n SBS-layers) concept, where each layer is composed of three sub-layers: the shear layer, bending layer, and spring layer. Expanding on the SBS differential formula, Zhao et al. [47] proposed model types tailored to various superstructures along with their mechanical parameters. Additionally, by integrating the Terzaghi model addressing seepage consolidation, they asserted that the Winkler–Terzaghi model effectively addressed the challenge of soil discontinuity.

2.2. Elastic Half-Space Model

The elastic half-space model is anchored by three translational springs and three rotational springs, with added dampers to account for soil damping and replicating the deformation behavior of the surrounding soil. In light of this, SSI predominantly involves motion interaction and inertia interaction. In instances of high seismic intensity, the impact of inertia interaction takes precedence. Therefore, selecting an appropriate foundation resistance function becomes crucial in accurately characterizing the inertia interaction [48].

Except for the ring augmented by Veletsos and Tang [49], Gazetas [50] provided impedance functions for nearly all foundations, all based on homogeneous soil. Chen [51] introduced the impedance function for layered foundations, employing the Cone model, which essentially substitutes a cone with a specific tensor angle for the semi-infinite body. As earthquakes involve multiple frequencies of seismic waves superimposed, utilizing the parameters suggested by Gazetas [50] directly for calculating dynamic stiffness and damping [52] may not be viable. Instead, more precise algorithms are essential to address the nonlinear behaviors of SSI.

2.3. Finite Element Method (FEM)

The finite element method (FEM) stands out as one of the most effective ways to depict SSI, given its capacity to accurately replicate nonlinear soil behaviors [45]. Therefore, this subsection explicitly details both FEM and its derived methods. To enhance accuracy in FEM, three critical aspects must be considered: the soil constitutive model, artificial boundary conditions, and mechanical properties of contact interfaces. While the previously discussed substructure method also addresses the assessment of Foundation Input Motion (FIM) [43] in the free field, it is crucial to note that FEM, by simulating the variation of soil as seismic waves traverse the site, demands special attention to the input mode of the seismic wave, particularly concerning the artificial boundary. The soil constitutive model is typically categorized into linear–elastic, elastoplastic, and viscoelastic models. The linear–elastic model, based on the generalized Hooke’s law, is straightforward but has limitations, such as its inability to describe hysteresis, nonlinearity, and dynamic response deformation accumulation in soil [53]. To address the above limitations, the elastoplastic model, with its primary objective of articulating variation curves for the shear modulus ratio and damping ratio [54], incorporates yield criteria, the flow rule, and hardening rule [55]. Viscoelastic models are divided into two elementary branches: the equivalent linear model and the time–domain hysteretic nonlinear model. To linearize the nonlinear problem, Seed and Idriss [56] initially introduced the equivalent linear model, substituting the equivalent shear modulus and equivalent damping ratio for the original ones. Despite its simplicity and applicative advances, this model is restricted by soil strain and seismic acceleration [57]. For typical constructions, the region where strain exceeds the critical value is usually within a certain fraction of the foundation width on both sides [58]. The shear strain in this part can be adjusted to enhance the calculation accuracy [59]. Masing’s nonlinear constitutive model, first proposed in 1926 [60], has undergone modifications to produce various types of Masing models, with notable examples being the Hardin–Drnevich [61] and Ramberg–Osgood [62] models. Subsequently, Martin and Seed [63]

established the Davidenkov model, presenting a calculation method following Masing's rules [64]. Based on the double criterion, Pyke [65] proposed the multiple rule, which has been implemented in the Masing model.

When employing FEM, it is essential to implement artificial boundaries that simulate the radiation damping of an infinite foundation. This serves the purpose of transforming an unbounded domain into a bounded one, thereby preventing the reflection of scattered waves at the interception boundary [66]. Global and local artificial boundaries are two categories of artificial boundaries [67]. The former, including the infinite element method (IEM) [68], BEM, etc., offers high levels of precision but is computationally intensive. The other consists of a viscous boundary [69], paraxial boundary [70], Higdon boundary [71], transmission boundary [72–74], viscous-spring artificial boundary [75], and so on. Among these viscoelastic boundaries, which exhibit excellent precision and stability in handling both static and dynamic problems [76], have been shown to consider both the large-scale basin effect and local nonlinear effect [77]. Also, it is one of the artificial boundaries recommended by the seismic design of nuclear power plants in China [75].

Seismic input can be categorized into three methods, namely the displacement input [78], acceleration input [79], and seismic motion input [80]. Since seismic motion input is derived from the viscoelastic artificial boundary, which has a greater fit, it is prioritized while employing the viscoelastic boundary [81]. This method works when the seismic wave propagates in a single homogeneous field [82]; however, it is less effective if the seismic wave traverses two or more soil layers with differing wave impedances. For dealing with this problem, there are generally two methods: the frequency [83] and the time [84] domain method. Although the former is more exact [85], its application in intricate foundations is incalculable. To derive the equivalent input seismic load of the artificial boundary, researchers employ SHAKE91, DEEPSOIL, EERA, etc., learning from the substructure method [86].

The contact interface refers to the soil mass adjacent to the structure with a thickness of 5~10 times the average particle size [87], the mechanical properties of which are intricate, affected by normal stress, structural surface roughness, the particle size of sand, sand type, and homogeneity coefficient of the soil particles [88]. There are three broad approaches to thinking about the contact interface: the shear tests for empirical formulas, soil constitutive model, and mechanical model of contact interface that can be more accurate than the former [89]. For creating an interface model, there are two mainstream methods [90], either utilizing functional equations (Lagrangian or Penalty function) to turn the contact problem into non-contact or establishing a constitutive model of contact element [91], including the zero-thickness Goodman element [91] and Desai thin-layer element [92]. The former element serves when shear failures occur at the contact interfaces, while the other is employed in a situation where shear failure happens to the nearby soil.

As previously stated, for FEM, when the infinite or semi-infinite field is estimated, it is necessary to construct a large large-size mesh structure to simulate the near-field and an artificial boundary is set to absorb the seismic waves from the far-field [93], which may generate a large computational requirement for some large-size models, whereas the boundary element method (BEM) only necessitates the establishment of the mesh of the contact interface between the foundation and the soil. Hence, one of the ways proposed to facilitate the resolution of the dynamic response of the SSI with a complex contact surface is the finite element method–boundary element method (FE–BE coupling method) obtained via introducing BEM based on FEM. The FE–BE coupling method is a method for calculating the superstructures and soil foundation following different methods. Generally, BEM is used to simulate the dynamic behavior of layered soils [94,95], while FEM is employed for superstructures. In some circumstances, only the far-field is calculated using FEM, which is defined as the scaled-boundary finite element method (SBFEM) [96].

The primary objective of BEM is to address Laplace's equation, facilitating the conversion of integral equations within the boundary region of the far-field and the SSI system into boundary integral equations [97]. Once the boundary has been discretized via fre-

quency [98] or time domain [99] methods, the simplified dynamic response equation can be derived [93].

The wave propagation in unbounded fields has been effectively modelled in both the time and frequency domains using the semi-analytical stiffness-based finite element method (SBFEM) [100]. SBFEM stands out due to its exemption from artificial boundary conditions or the fundamental solution requirement, a characteristic not shared by the boundary element method (BEM). This allows seamless coupling with the near-field through the finite element method (FEM) and compensates for the limitations of BEM in mimicking anisotropic soil behavior [101]. SBFEM also generates symmetric dynamic stiffness and unit impulse response matrices, improving computing efficiency [102]. In the extension of the sequential boundary field element (SBFE) to model three-dimensional layered soils, Birk [103] suggested employing a scaling line rather than a proportionate center point. Furthermore, an alternative approach, the indirect boundary element method (IBEM), has been proposed for assessing the seismic response of anisotropic soils [104].

3. Advances in Numerical Simulations on SSI

3.1. Site Effect

The topography and soil properties of a site have discernible impacts on SSI, with the latter playing a pivotal role [105]. When soil nonlinearity is taken into account, the effects of SSI and SSSI extend to a broader range of applications, surpassing the scope covered by the linear elastic model [106].

The propagation of seismic waves within a field varies based on soil properties. Typically, dense soil tends to amplify seismic waves [107], while soft soil may exhibit a similar effect or act as a filter. However, relying solely on soil properties for estimates is inherently inaccurate. The filter effect was exemplified by the softening of soil and the deceleration of waves, as observed in Chen et al.'s investigation into the impact of nonlinearity on SSI [108]. In this study, the arrival time of seismic waves was delayed at the free surface due to the filter effect. It is noteworthy that calculations solely based on soil properties may lead to inaccuracies, especially considering the interlayer reflection coefficient is less than 0 for the weak layer at the bottom, potentially resulting in a transition from forward displacement to reverse displacement. To substantiate the amplification effect of weak soil, Chen et al. [23] conducted an assessment of the seismic response in areas with varying shear velocities (V_S). Their findings indicated that the amplification coefficient of surface acceleration decreased with an increase in the seismic intensity. This trend was attributed to heightened ground motion, which accentuated soil nonlinearity [109]. Notably, not all amplification factors exceeded 1, particularly in cases where the soft soil thickness was less than 4 m. For instance, when the coverage thickness exceeded 6 m, this was verified through both centrifugal simulation [107] and seismic analysis at an actual site [109]. However, the amplification factor was also contingent on the distribution of the weak layer. If a thin, weak soil layer was situated on top of the field, ground acceleration would be exacerbated. In cases where the soft soil was positioned in the middle, its role could vary depending on the depth of burial and thickness. A deeper and thicker layer might act as a seismic isolation layer, while a shallow and thin weak layer could produce the opposite effect [109]. It is crucial to emphasize that, analogous to the phenomenon observed in the 1923 Kanto Earthquake [110], excessively violent ground motion, leading to soil degradation, could result in the dramatic failure of the weak layer, significantly amplifying surface acceleration.

As outlined in [54], a slope devoid of a soft layer demonstrated an amplification effect on vertical ground motion. However, the impact predicted using a nonlinear model, characterized by greater energy consumption, was found to be less significant than that determined using a linear model. The amplification coefficient of ground motion exhibited a decrease correlating with a reduction in the shear wave velocity of the overlying soil, aligning with prior research findings. Notably, it is essential to recognize that the compressive modulus resulting from vertical earthquakes is considerably less than the

shear modulus. Despite this, it is crucial to note that the effects of soil nonlinearity on the propagation of P waves in soil are often overlooked. Nevertheless, previous studies have demonstrated that soil exhibits nonlinearity under the influence of strong vertical earthquakes [111]. Shahbazi et al. [112] conducted a comparative analysis of the impact of soft and hard soil on the seismic responses of superstructures, yielding results consistent with those aforementioned. Incorporating SSI considerations, flexible structures built on hard soils were estimated more conservatively. However, it became evident that SSI could not be overlooked when assessing structures characterized by higher stiffness situated on a soft foundation. Furthermore, the dissipative effect of the weak layer proved advantageous in the seismic design for superstructures, particularly when hard soil was positioned above a suitable soft layer capable of supporting the structure without undergoing considerable settlement or liquefaction.

Considering the most unfavorable site conditions, the subsequent review will focus on the numerical studies of the seismic responses of the structures erected on soft soil.

To compare the seismic responses of a structure before and after the involvement of soil, Xu et al. [113] constructed a 15-story concrete building using FLAC 3D considering different shear strengths and ground motions, as illustrated in Figure 1. Within the range of shear strengths considered in this study, the computational results revealed that SSI significantly amplified the maximum base shear, lateral displacement, and inter-story drift. Notably, when the shear strength of the soil was elevated from 65 kPa to 105 kPa, the influence of SSI on the maximum base shear, lateral displacement, and inter-story drift increased by 60%, 100%, and 44%, respectively.

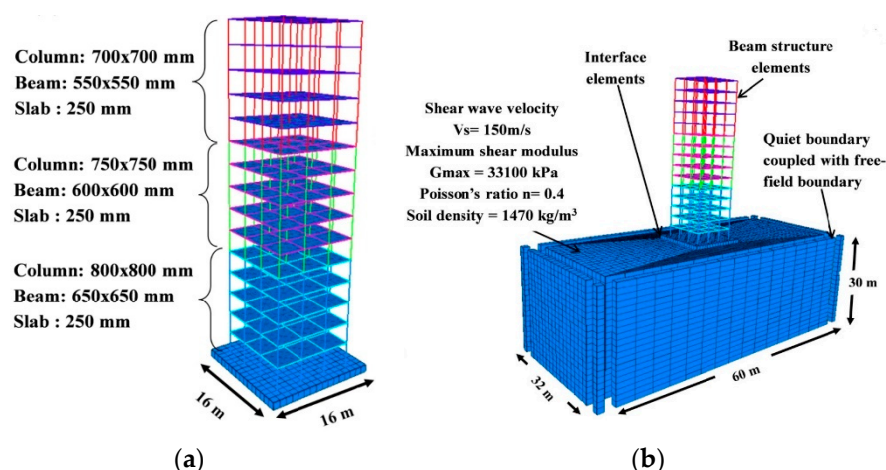


Figure 1. 15-story flexural concrete structure without and with considering SSI [113]: (a) fixed-base model; (b) SSI model.

Mercado et al. [114] conducted a comparative analysis to assess the impact of linear and nonlinear fields on SSI, as depicted in Figure 2. The results indicated that the SSI effect primarily manifested in an increase in the peak horizontal acceleration of the structure. When compared to the results calculated using the linear model, the nonlinear model exhibited a decrease in the peak acceleration and inter-layer drift of the superstructure, implying that the application of a linear model might be overly conservative. Previous research has also underscored that the error of the equivalent linear model grows with the increment of the site period [59].

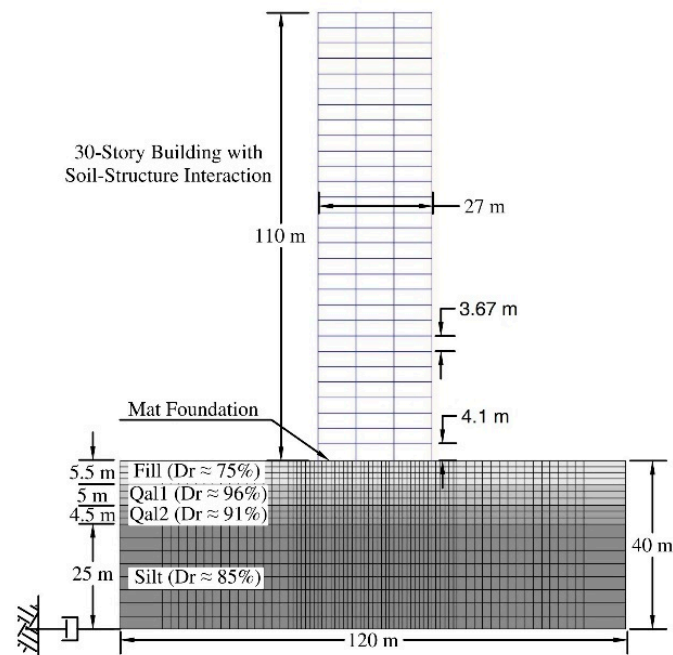


Figure 2. Finite element model of the tall buildings considering SSI [114].

In specific scenarios, particularly when a building is designed in proximity to a slope, the TSSI effect cannot be overlooked. Alitallesh et al. [29], utilizing FLAC 3D, simulated a model as shown in Figure 3 to investigate the influences of soil and slope conditions on both SSI and TSSI. The results indicated that the SSI and TSSI effects were more pronounced when the upper overburden soil layer (h_1) was thinner. Notably, in cases where a soft layer overlays a hard layer, seismic waves were amplified in the upper layer, further affirming the findings observed by Chen et al. [23] in uneven terrains. Additionally, it was revealed that the impact of the slope height on TSSI was more substantial than that of the slope angle. Moreover, when assessing the SSI effect in soils with varying shear wave velocities, it was observed that SSI could be disregarded for flexible superstructures with rigid foundations, aligning with the conclusions drawn by Shahbazi et al. [112].

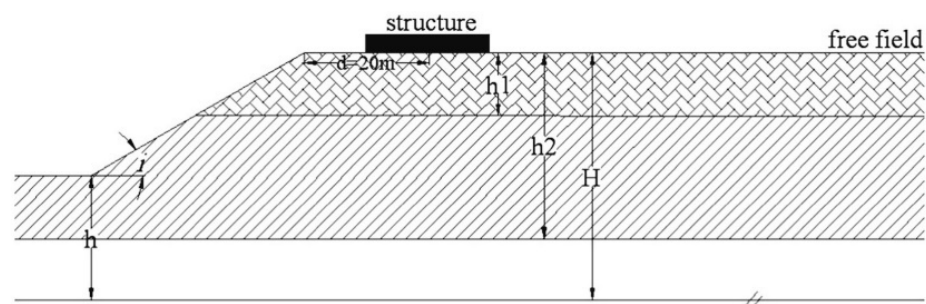


Figure 3. Illustration of TSSI with stratified soil layers [29].

Through adjustments to the geological parameters, slope angle, and slope height, Erfani et al. [115] examined the TSSI and its impact on the seismic response of structures. Their study revealed that slope stiffness decreased with an increase in slope angle, resulting in a simultaneous increase in structural inter-story drift. The effect of the seismic waves reflected by the slope on the structure diminished as the structure moved farther from the slope border. However, although the extra vertical seismic waves generated by the reflection also decreased, the interlayer drift increased, resembling the SSI effect. Notably, when $V_s = 150$ m/s, the influence of TSSI approached that of SSI, illustrating that the contribution of soil properties to SSI was more significant than that of topographic conditions.

Shamsi et al. [116] applied MIDAS GTS/NX to develop the model of SSI, TSSI, and TSSSI, as shown in Figure 4. In this study, a 15-story steel frame was adopted as the benchmark model, and the influences of various parameters were investigated, including the slope height (H), the distance of the structure from the slope (X), the angle of the slope (i), and the distance between the two structures (D). Studies have demonstrated that the effect of X was greater than that of the soil condition, i and H . When numerical simulation results of SSI and TSSI models were examined, it turned out that the slope effect could essentially be omitted when X/H exceeded 2.5~5, and the ratio that referred to the H and soil parameters was more conservative in comparison to earlier research [27]. Where the ratio of inter-story shear and displacement of TSSI and SSI superstructures was more than 1, attributed to the difference in soil shear wave velocity, the precise amplification coefficient still had to be determined based on site conditions. According to the numerical simulation results, TSSSI had more serious damage on the structure immediately adjacent to the slope, triggering the structure to move towards the slope, but this impact is only cause for concern when $D \leq 0.5a$, while the slope effect of the structure far from the slope could be barely noticeable when $D = 0.5a$.

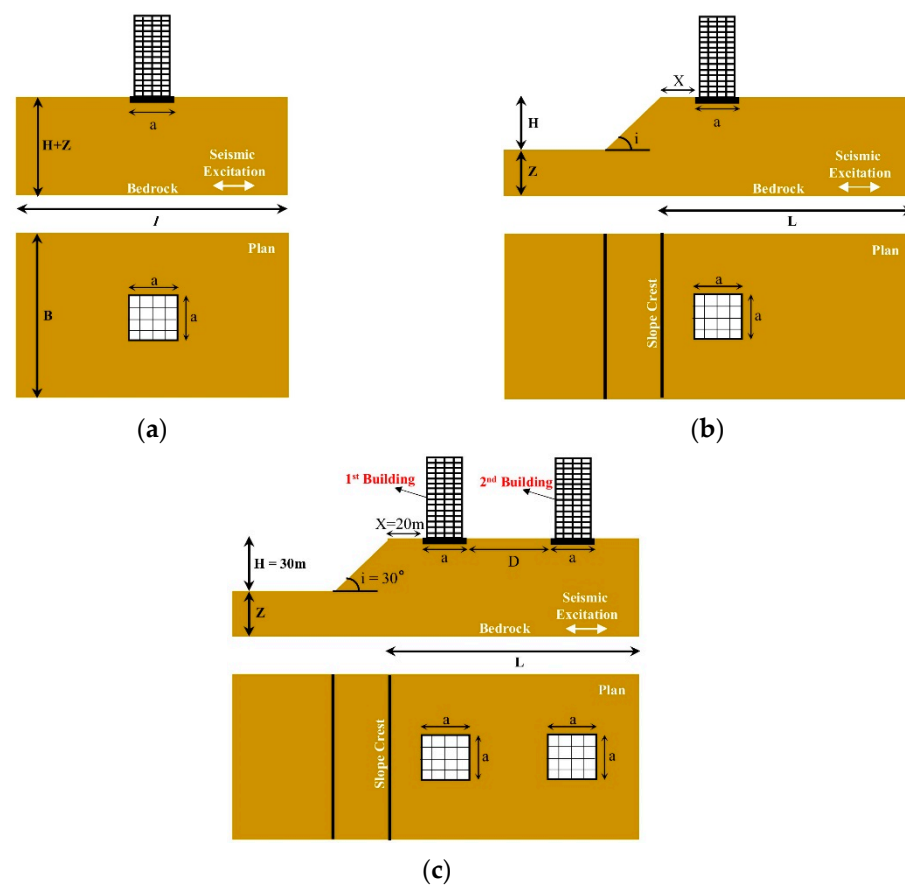


Figure 4. Illustration of SSI under different terrain conditions [116]: (a) SSI; (b) TSSI; (c) TSSSI.

3.2. Seismic Excitation

Seismic acceleration amplitude, vibration frequency, displacement direction, and incident angle constitute the primary factors influencing SSI. In the context of selecting seismic waves, Zhan et al. [117] conducted a study examining the impact of large-scale soft sites subjected to far-field earthquakes. The findings revealed a noticeable prevalence of long-period ground motion in such scenarios. In contrast to artificial waves, the amplification effect on ground motion caused by far-field large earthquakes in large-scale soft sites appeared more pronounced, with the amplification coefficient increasing alongside the ground motion intensity. This observation diverges from the conclusions drawn by

Chen et al. [23] based on previously used amplification coefficients, possibly attributed to variations in the spectral composition of seismic waves. An optimized algorithm, as proposed by [118], can effectively determine the site period as follows:

$$T = \sqrt{\sum_{i^{th}}^N \left(\frac{4h_{i^{th}}}{v_{i^{th}}} \right)^2 \frac{2H_{i^{th}}}{h_{i^{th}}}} \quad (1)$$

$$H_{i^{th}} = \sum_{n=1}^{i^{th}} h_n - \frac{1}{2}h_{i^{th}} \quad (2)$$

where $h_{i^{th}}$ is the thickness of the i^{th} soil layer, $v_{i^{th}}$ denotes the shear wave velocity of the i^{th} soil layer, $H_{i^{th}}$ presents the midpoint depth of the i^{th} soil layer, and N signifies the total number of soil layers, illustrated in Figure 5. The deep soft soil site with a longer period (1.13~1.28 s) amplified the far-field vibration with a similar peak spectral period, whereas it significantly filtered the ground motion with a larger peak spectral gap (shorter period less than 0.3 s or larger period more than 2.5 s). Subsequent investigations have indicated that distinct seismic waves exhibit comparable effects on a given SSI model when adjusted to the same amplitude and selected based on the response spectrum [59].

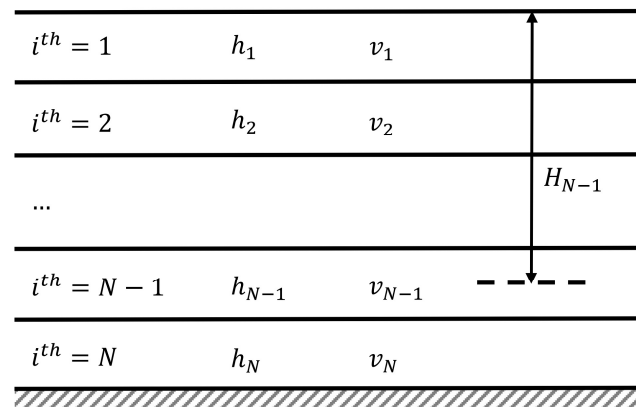


Figure 5. Illustration of the horizontally layered site.

Beyond the amplification of unfavorable stability given the similarity of the soil and seismic wave period, when the frequency of the foundation and superstructure matched that of the seismic wave, it could induce a worse situation, where the structure resonated as a seismic response and reached its peak. Especially for frame construction [119], the destruction of the substructure would be worse than that of the pile foundation. Citing ref. [120], if the seismic wave was an oblique wave incident, the superstructure could resonate at a certain frequency owing to phase fluctuation, which correlated to the stiffness ratio of the foundation and soil or superstructure. When the pile foundation was in a sedimentary clay layer, the foundation stiffness was significantly higher than that of soil, resulting in the vibration of the upper frame by the long-period motion of the ground rather than with the basic period of the foundation. Ergo, the displacement of the pile foundation did not originate from the vibration caused by the upper structure but rather from the soil driving, creating quite low interlayer displacement and damage. The displacement between the superstructure and the foundation was smaller the higher the damping ratio of the superstructure was [112]. Furthermore, the looseness of the backfill layer opposed to the original soil could trigger the surface ground vibration to be further exacerbated [31].

In addition, Zhou et al. [121] investigated the seismic behavior of a concrete chimney under multidimensional earthquakes. It was observed that the structure would be more vulnerable under three-dimensional ground motion than under one-dimensional or two-dimensional ground motion. Meanwhile, the incidence angle would have an impact on the seismic response of the SSI, especially in the case of major earthquakes, which would not be insignificant due to the smaller foundation size, and the most unfavorable input angle is 45°

when the PGA is greater than 0.2 g. Dams [122] and frame structures [123] experienced a similar situation, although considering the type of seismic wave, the thickness and qualities of the soil, etc., the unfavorable angle may be larger or less than 45° . Hua [124] reached an analogous conclusion following research of the field under the action of 3D seismic waves that both the thickness of the soil layer and the angle of the incident wave affected the surface amplitude. They would be at maximum when the SH wave was incident perpendicular to the plane in which the P wave and SV wave reside, which was roughly fourfold the incident amplitude when the P wave was incident at an angle of 36° and the SV wave was at an angle of 54° . He further noticed that when the soil layer thickened, the surface amplitude climbed, and then fell, and then returned. Notably, the influence of vertical ground motion on foundation–structure settlement is virtually negligible unless the frequency of the vertical ground vibration approaches the resonance frequency. The nonlinearity introduced in the soil due to vertical motion is also less pronounced compared to that induced by horizontal motion [125].

3.3. Foundation Form

The stiffness of the foundation significantly influences the SSI effect, with the dynamic response at the interface between a flexible foundation and superstructure typically surpassing that of a rigid foundation below [120]. The emphasis on analyzing soil and pile–soil contact in seismic response studies stems from the notable impact of nonlinearities in soil properties and pile–soil interfaces, which often outweigh those associated with superstructure materials [126]. Wu et al. [126] observed that the soil adjacent to the pile tip and pile side exerts varying effects on the seismic response of the superstructure, with the former significantly influencing higher-order modes of the structure and the latter affecting lower-order modes more prominently. Additionally, Zamani and Shamy's study [125] on the soil beneath the foundation revealed that the acceleration amplification factor of the soil beneath a rigid foundation exceeded that of the free field at the same depth, indicating an adverse effect of the foundation on soil motion.

Previous studies on seismic predictions for structures have demonstrated that the inclusion of SSI alters the internal force distribution within the foundation [108]. Consequently, the amplification or reduction factor for the same structure under different foundations varies compared to assumptions made for a rigid foundation. Hokmabadi and Fatahi [19] assessed the sensitivity of foundations to SSI using FLAC 3D. The findings are summarized as follows: (a) the SSI effect effectively reduced the base shear, with the degree of influence being higher for the pile–raft foundation and pile foundation models than for shallow foundations; (b) the maximum sway angles for pile foundations and pile–raft foundations were, on average, 44% and 54% smaller than those for shallow foundations. The sway angles were attributed to the inertial force of the superstructure under seismic forces, causing settlement on one side of the foundation and bulging on the other; (c) the SSI effect exhibited clear amplification of lateral deformation and interlayer displacement, though the amplification was less pronounced for pile foundations and pile–raft foundations compared to shallow foundations. Furthermore, the study revealed that soft soil responded differently to various seismic waves. For instance, under low and medium acceleration, soft soil demonstrated a noticeable amplification impact on seismic waves. However, under excessively large acceleration, the soft soil inhibited the propagation of seismic waves towards the soil surface.

To explore the impact of the foundation type on the seismic response of a mid-rise building considering SSI, Zhang and Far [127,128] created two different foundation types, the end-bearing piled foundation, and classical compensated foundation, as shown in Figure 6. When the shear wave velocity was 150 m/s or 320 m/s, it was demonstrated that the SSI effect magnified the interlayer shear of the piled foundation-supported structure, and yet, for soil with $V_S = 600$ m/s, the SSI effect was not obvious, and the amplification factor was even less than 1. When a structure is erected on soft clay ($V_S = 150$ m/s or 320 m/s), the use of a compensated foundation makes it more vulnera-

ble to ground motion. The SSI effect substantially hinders the dynamic response of the structure. Additionally, the interlayer drift experiences significant amplification when SSI is considered for both pile and compensatory foundations. This observation aligns with the findings of Tabatabaiefar et al. [129], namely that SSI had a pronounced effect on the inter-story drift of frame structures.

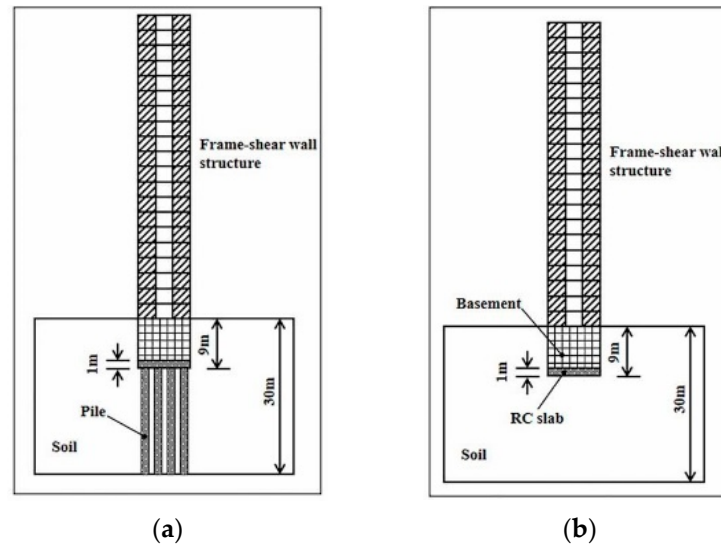


Figure 6. Models of frame-shear wall buildings considering SSI [128]: (a) end bearing piled foundation-supported structure; (b) classical compensated foundation-supported structure.

3.4. Superstructure

Computational models developed by Monsalve et al. [130], as depicted in Figure 7, reveal that the SSI effect enhances the inter-story drift ratio and acceleration of high-rise buildings. Simultaneously, it extends the period of low-order modes with minimal impact on high-order modes. Furthermore, it is noteworthy that the inclusion of a shear wall can, to some extent, mitigate the increase in inter-story drift while facilitating the expansion of story acceleration.

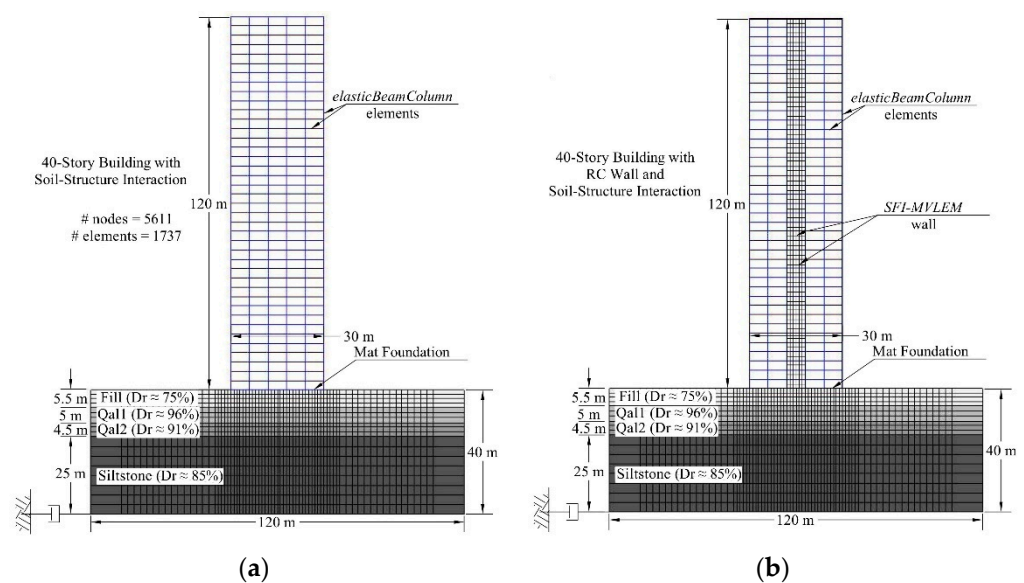


Figure 7. Models of the tall buildings without and with shear walls considering SSI [130]: (a) a building model; (b) a building model with shear walls.

In the study conducted by Mercado et al. [131], the results underscored the significant influence of the structure's geometry and the shear wave velocity of the soil on the lengthening of structural periods induced by the SSI effect. Notably, structures with larger aspect ratios and foundations in looser soil exhibited a more pronounced extension of periods. These findings align with observations in 1999, where Stewart et al. drew similar conclusions based on an analysis of 77 strong-motion data sets collected from 57 construction sites [132]. They measured the response of the SSI effect on structure in terms of the first-mode period lengthening ratio, \tilde{T}/\bar{T} (\bar{T} denotes the first-mode period without soil modelling, and \tilde{T} denotes the first-mode period with SSI), and their observations revealed that the dimensionless ratio of structure–soil stiffness $1/\sigma$, was the most significant influence factor of \tilde{T}/\bar{T} , which could be expressed as

$$1/\sigma = \frac{\bar{h}}{V_S \cdot \bar{T}} \quad (3)$$

where \bar{h} denoted the effective height of the structure. Other parameters, including the structural aspect ratio, foundation type, etc., were negligible.

To investigate the sensitivity of structures with various parameters to distinct soils under the action of four different seismic waves, Zhang and Far [128] established frame structures with a range of stories (20, 30 or 40 floors) and height-width ratios ($HWR = 4, 5, 6$), as shown in Figure 8. Their findings stated that the rise-span had a minor impact on SSI, but the story height could not be omitted. Iida et al.'s survey on steel-framed and reinforced-concrete-framed structures located in Tokyo Bay [119], where resonance occurred due to the proximity of the periods, might help to explain the phenomenon that the latter effect increased nonlinearly and the mid-rise building was more susceptible to the SSI effect than the low-rise and high-rise building.

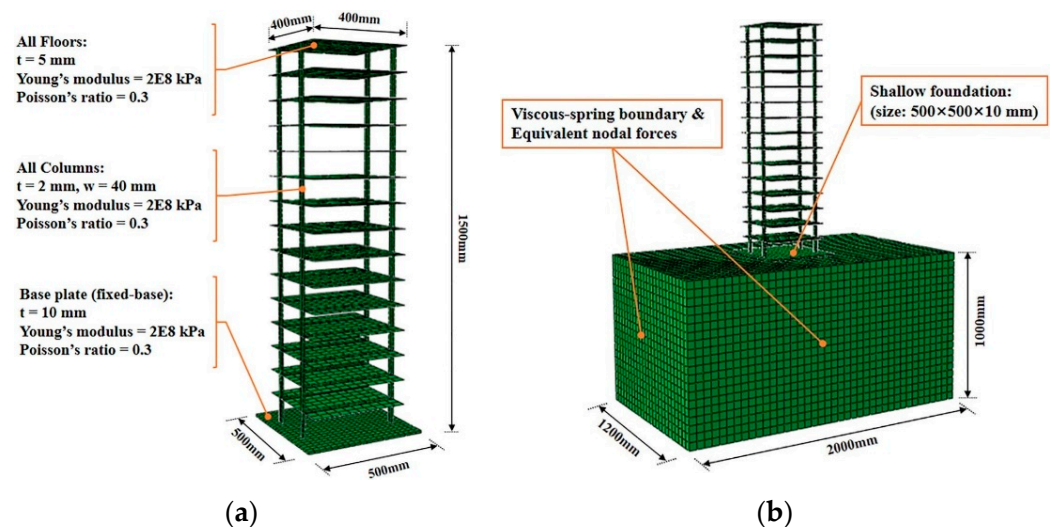


Figure 8. Numerical models with and without considering SSI [128]: (a) fixed-base model; (b) flexible-base model.

Similar to Alexander et al. [133], Liang et al. [134] found that the SSSI effect might alter the structural response at specific frequencies by 30~50%. Their simulation, utilizing the integral equation boundary element method (IBEM) in two dimensions, indicated that when the limit was surpassed, a building could be treated as an individual entity, with the scaling factor contingent on the distance between structures. The study made it clear that the distance between structures significantly impacted the scope and magnitude of the SSSI effect, persisting even when two flexible foundations were spaced up to 10 times their respective radii apart [120]. This finding is consistent with Iida's investigation into the

1985 Michoacan, Mexico, earthquake [135]. Additionally, Vicencio and Alexander's [106] research confirmed that the influence of SSSI could be disregarded in conventional seismic calculations when the distance between structures exceeded almost twice the foundation size. However, the significance of this observation was not definitively tied to soil properties; the lower the shear wave velocity of the soil, the greater the ratio [116].

Another crucial factor influencing the SSSI effect is the height ratio between structures. In Vicencio and Alexander's study [106], SSSI exhibited a significant amplification effect on the lower building, potentially reaching 400%, while causing a suppression effect of nearly 50% on the taller building, especially when the height ratio between the two structures exceeded 1.5 times. Farahania et al. [136] further emphasized this principle, stating that the seismic response of low-rise buildings could be effectively mitigated by increasing the net distance between structures. However, for high-rise buildings, this effect was deemed negligible as the SSI effect was much more intense than the SSSI effect.

Following converting one of the models from the Trombetta et al.'s [137] tests on the SSSI effect in urban neighborhoods (cSSSI model) into a prototype structure with a scaling factor (1:55), as illustrated in Figure 9, Bolisetti and Whittaker [138] carried out a numerical analysis. The simulated structure exhibited that when the combined arrangement was performed in the cSSSI model, SSSI failed to impact the global seismic response of the low-rise and mid-rise structures. In contrast, the SSSI did affect the peak acceleration response of the foundations, particularly in the presence of a deep foundation, which had a restraint effect on the neighboring low-rise building with shallow foundations. In Section 4.3, the experimental results that correlate to this numerical simulation will be enumerated.

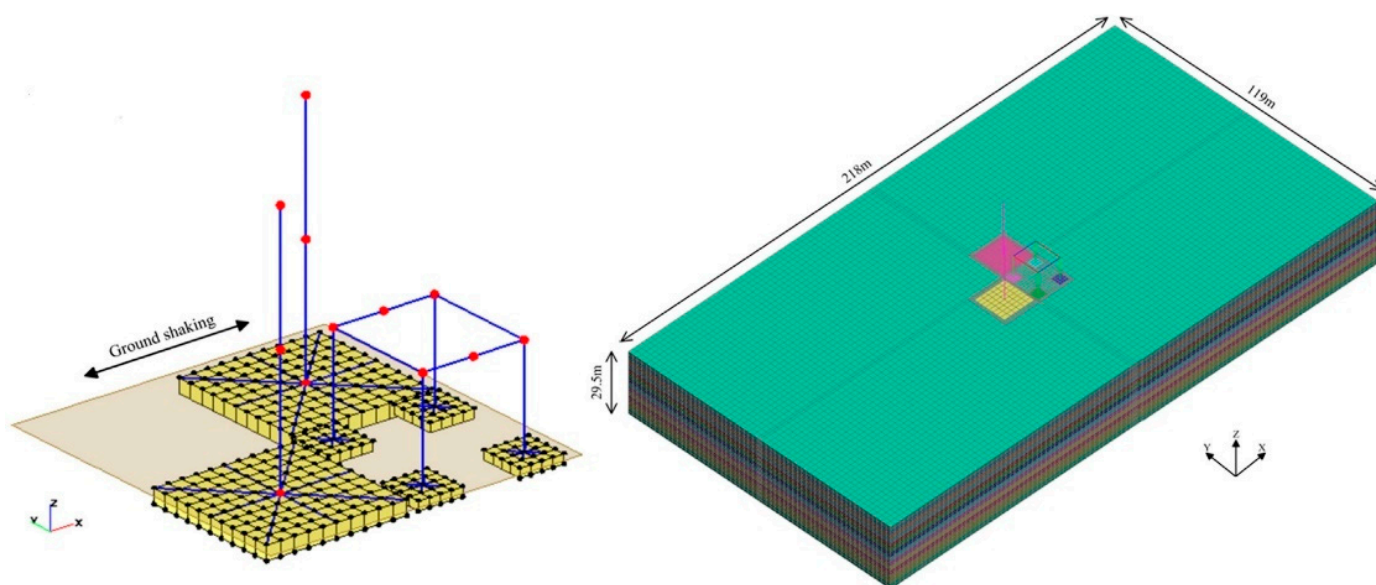


Figure 9. Numerical models of the cSSSI arrangement in SASSI (left) and LS-DYNA (right) [138].

To assess the influence of SSSI on the extensive clusters of buildings, Vicencio and Alexander [139] introduced a simplified reduced-order model illustrated in Figure 10. The findings indicated that while the SSSI effect on structures located at the corners was not maximized, it did amplify the seismic response of structures parallel to the excitation orientation.

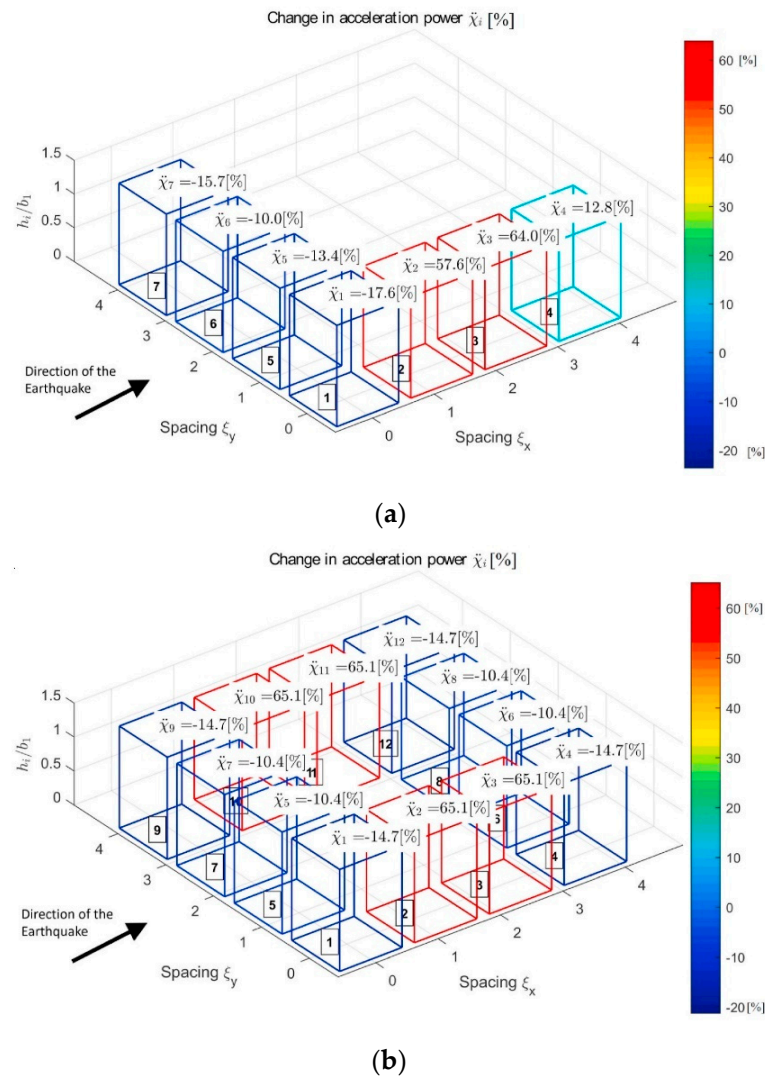


Figure 10. Change in acceleration power due to 3D SSSI [139]: (a) L shape arrangement; (b) a city block of twelve equispaced identical buildings.

4. Advances in Experimental Studies on SSI

4.1. Site Effect

Rayhani and Naggari [140,141] conducted vibration tests on a rigid structure at a depth of 30 m (1:80 scale) using the C-CORE 5.5-m radius beam centrifuge. That rigid structure was deemed to be a reasonable simulation of a 10-story building. The experimental setup included transducers for settlement measurement and accelerometers, as depicted in Figure 11. Glyben clay was employed during the tests to investigate the influence of soil shear strength on SSI effects. The undrained shear strength of the clay (RG-01) in Figure 12a was 40~60 kPa, with an average shear wave velocity of 73 m/s. The undrained shear strength of the clay (RG-02) in Figure 12b was 40~50 kPa for the top, and 85~95 kPa for the medium, with an average shear wave velocity of 100 m/s. Through a sturdy container, the superstructure was embedded in the clay. The results revealed that the SSI effect amplified the surface peak acceleration significantly, especially in instances of a minor input seismic amplitude. Furthermore, uniform clay (RG-01) amplified structural acceleration less than layered clay (RG-02), but RG-01 amplified near-surface acceleration over RG-02, which might be the consequence of the nonlinearities of the deeper and weaker clay. Also, when the seismic intensity increased, the amplification coefficient of the SSI effect on the amplitude and spectrum of seismic acceleration was minimized allowing researchers to hypothesize a connection between the degradation of the shear modulus and

the rise in soil damping under extreme vibration. The acceleration of the free field and clay near the surface under the structure is slightly smaller than the experimental results in the period of 0.2~0.5 s, which might be owed to the rigid boundaries of the model that caused the computed SSI effect to be smaller. The experimental results matched well with those obtained using numerical simulations in FLAC 3D.

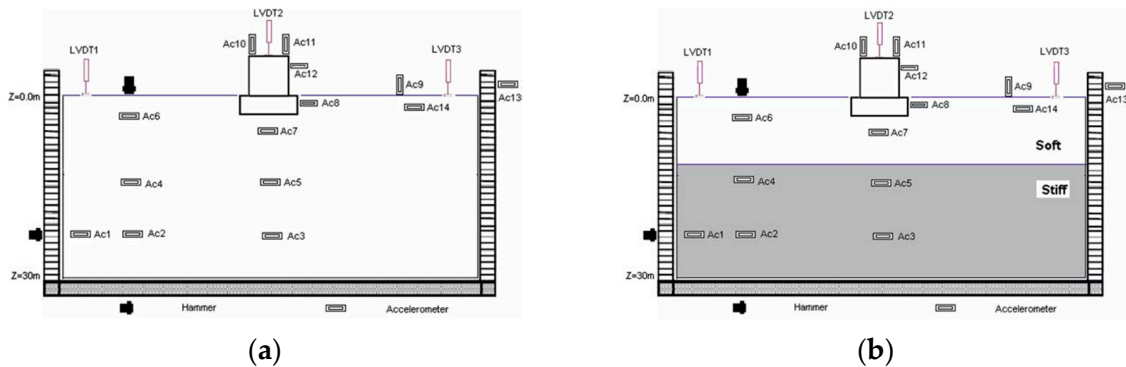


Figure 11. Centrifuge model configuration at prototype scale [140]: (a) Model RG-01; (b) Model RG-02.

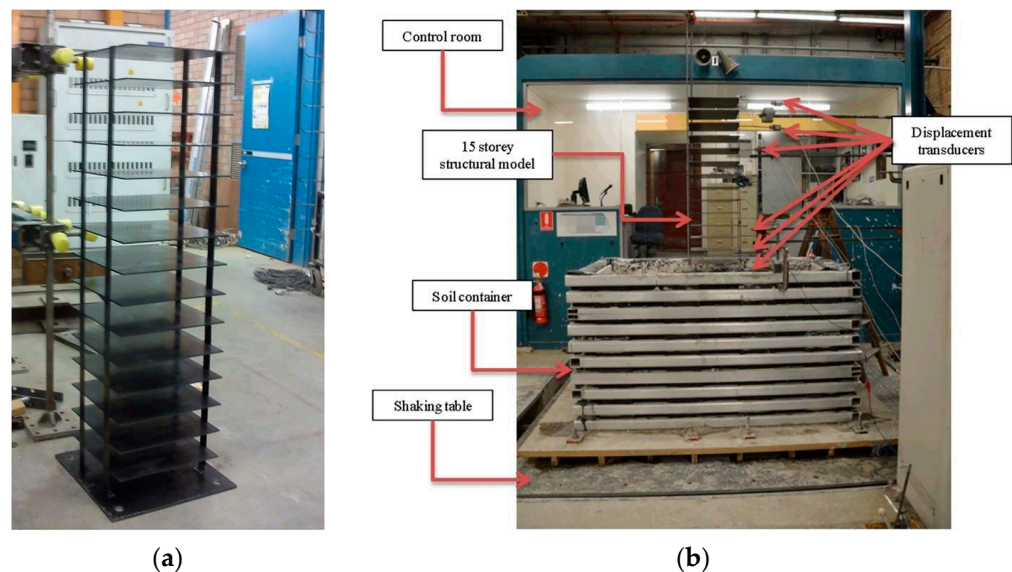


Figure 12. Models of shaking table tests [128]: (a) fixed-base model; (b) SSI model.

To compare the change in the inter-story shear of the same structure built on different foundations (rigid and soft), Zhang and Far [128] scaled a 15-story frame structure at a ratio of 1:30 and performed shaking table tests, as well as scaled a soil field with $V_S = 200$ m/s at the same ratio. The results revealed that SSI could not be ignored, especially when the shear wave velocity of the soil was lower. To validate the accuracy, the model developed in ABAQUS was compared with the findings obtained from this experiment.

Brennan [28] designed a TSSI centrifuge as in Figure 13, at a 1:50 scale to investigate the slope amplification factor under various conditions. The soil mass affected by TSSI occurred 0.31 H (the slope height was assumed to be H) longitudinally from the soil surface and 0.63 H from the lateral slope, according to the centrifuge test discoveries, with an amplification factor of roughly 1.5~2.0. The range of influence and amplification factors obtained from the experiment were found to be smaller than the numerical results, likely attributed to the errors in the scaled model and the distinct properties of the soil. Nonetheless, this experiment substantiated that the slope height significantly influenced the

TSSI effect, reinforcing the conclusions drawn from the numerical simulations. Additionally, the soil exhibited a filtering or amplification effect on seismic waves at various frequencies.

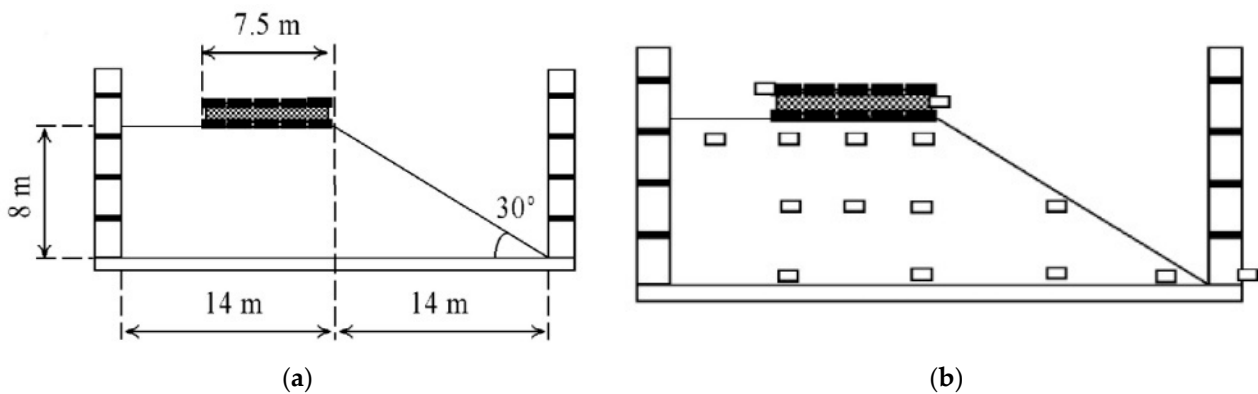


Figure 13. Experimental model of TSSI [28]: (a) dimensions; (b) accelerometer positions.

4.2. Foundation Form

Through shaking table tests, Shahbazi et al. [112] investigated the response of soil–pile–structure interaction under seismic action using a skid that mimicked the superstructure. The experimental setup consisted of two groups of four piles each, totaling eight helical piles, with distinct lengths and diameters in the two groups, as illustrated in Figure 14. The experiment spanned five days, with the seismic response of the pile group (featuring fixed and pinned connection types) measured during the final two days. The experimental findings indicated comparable seismic response characteristics for both connection types. Assuming a limit of 200 m/s for the soil shear wave velocity, the viscosity of the soil surrounding the piles was found to increase the shear wave velocity. Consequently, the stiffness and intrinsic frequency of the pile group were higher, resulting in a smaller displacement between the structure and piles. However, these effects could be disregarded when the wave velocity exceeded the threshold.

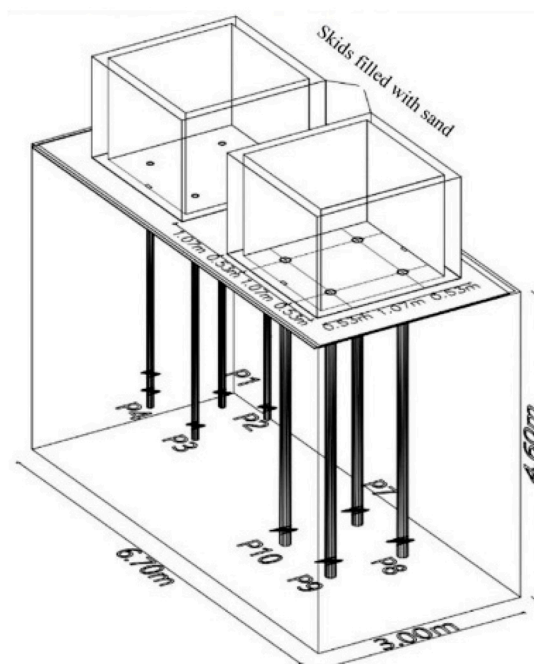


Figure 14. Schematic 3D view of pile groups and skids on shake table [112].

As depicted in Figure 15, Wang et al. [142] conducted a shaking table test on a six-story concrete frame at a 1:30 scale to assess the influence of the subsurface structure on SSI with varying foundation types, ranging from independent to box foundations. According to the experimental results, the SSI effects with the two different foundations caused a variation of up to 20% in the acceleration response of the soil. Due to the robust confinement provided by the box foundation to the superstructure, the overall acceleration response of the box foundation-supported structure was smaller than that of the independent foundation. However, the top layer of the box foundation exhibited a more pronounced amplification effect on the seismic response, characterized by a noticeable whiplash effect. Additionally, the researchers noted that the foundation type had a limited impact on the horizontal spectral characteristics of the structure but a more substantial influence on the acceleration amplitude and vertical spectrum.

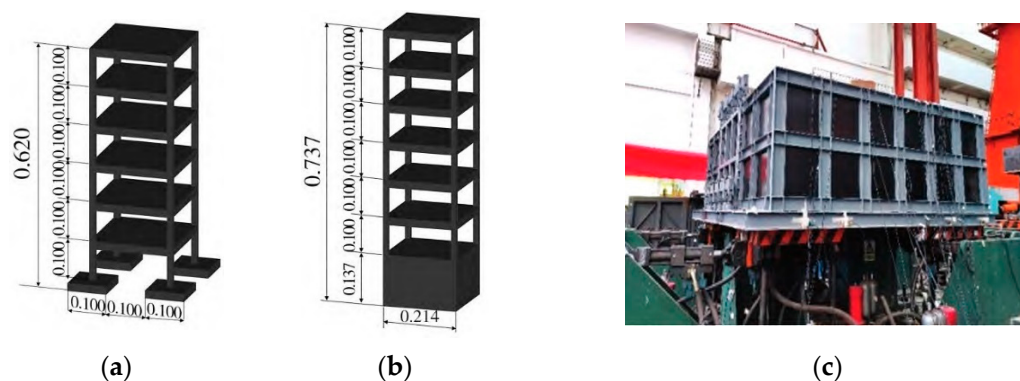


Figure 15. Superstructure diagram and test site [142]: (a) frame structure with independent foundation (unit: m); (b) frame structure with integral box foundation (unit: m); (c) soil container.

4.3. Superstructure

To assess the influence of soil–foundation–structure interaction (SFSI) and SSSI on the seismic response of structures, Trombetta et al. [137,143,144] conducted centrifuge experiments, as depicted in Figure 16. In Figure 16A, test-1 and test-2 were executed by adjusting the separation between two structures: a low-rise frame structure with a shallow embedded foundation and a mid-rise frame structure with a substantial basement. The tests affirmed that the SFSI effect indeed extended the period and increased damping. Moreover, the structure with a basement, capable of inhibiting permanent deformation, was found to be more susceptible to the SFSI effect. Test 2, on the other hand, demonstrated that the presence of deep footing influenced the moment–rotation behavior of the neighboring shallow foundations. As the constraints on shallow foundations increased, the system damping decreased, and the ratio of energy dissipated in superstructure vibration to the total energy dissipated increased. This scenario was less favorable for the seismic response of low-rise buildings. Building on the insights from Test 2, the researchers investigated the impact of SSSI on the seismic response of multiple structures by rearranging buildings. The findings indicated that for small and medium earthquakes, accounting for the SSSI effect was essential. With the intensification of ground motion, the nonlinearity of the SFSI increased gradually, while the SSSI effect diminished gradually, possibly due to a shift in the form of energy release. Additionally, this test confirmed that the vulnerability of structures to the SSSI effect depended on their nature and placement and was unrelated to the strength of the seismic wave.

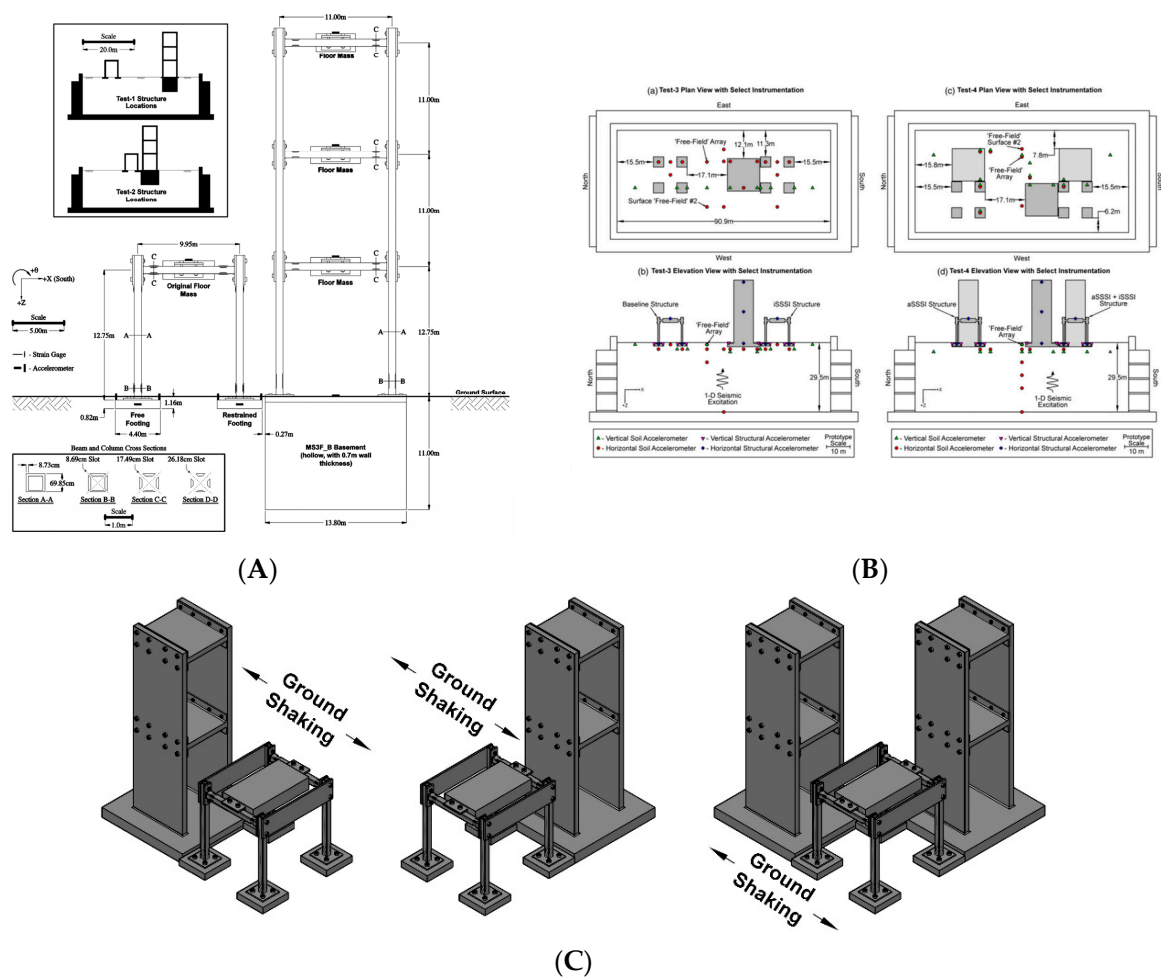


Figure 16. Shaking table test models of SFSI and SSSI: (A) setup of Tests 1 and 2 [143]; (B) setup of Tests 3 and 4 [144]; (C) diagram of iSSSI (Test 3), aSSSI (Test 4), and cSSSI (Test 4) (from left to right) [137].

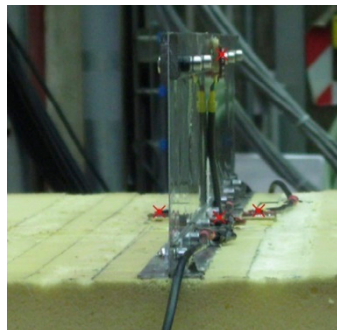
Aldaikh et al. [145] conducted a thorough investigation into the SSSI effects on three adjacent buildings through a shaking table test. To minimize the potential errors associated with genuine soil, a block cellular polyurethane foam was utilized, known for its linear and elastic propagation of seismic waves. In Figure 17b, the central building was replaced with an aluminium plate at the center of the foam box, while identical structures were installed on both sides, as depicted in Figure 17c. The test results indicated that the dynamic properties of the adjacent structures had discernible effects on the central building. Specifically, when the surrounding buildings were 10% to 20% higher than those at the center, the SSSI amplification coefficient on the seismic response of the central building could reach up to 170%. Conversely, when the surrounding buildings were 10% to 20% lower, the seismic response of the central building could be reduced by around 30%.

As depicted in Figure 18, Li et al. [146] reduced the scale of two 12-story cast-in-place concrete frame structures to 1:15, placing them on soft ground with a 200 mm separation. The test involved applying two seismic waves along the X and Y directions, and the impact of SSSI on the seismic response of the structures was assessed by varying the initial peak acceleration. The following conclusions were drawn from the test results: (a) the input excitation exceeded the acceleration response at the top of the free-field foundation; (b) as the initial excitation increased, the soil acceleration amplification coefficient, attributed to the combined effects of SSSI and SSSI, decreased and became similar in both the X and Y

directions; (c) at the pile–soil interface, a disparity in the amplitude of the contact pressure was observed, with greater values at the top or end of the pile and minimal visibility at the pile shaft.



(a)



(b)



(c)

Figure 17. Configurations of experimental models on shaking table [145]: (a) block cellular polyurethane foam (soil model); (b) central building model; (c) parallel buildings model.

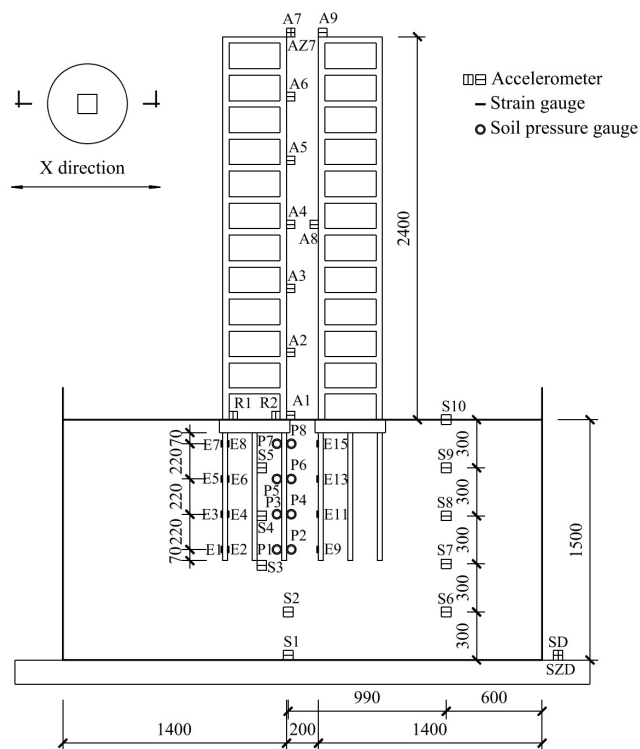


Figure 18. Geometry of model and experimental setup [146].

5. Research Advances on SSI for Large-Span Spatial Structures

In large-span spatial structures, the interaction between upper roofs and lower supporting structures is pivotal. The upper roofs act as a stiffness constraint on the lower structures, while the latter has an amplification effect on the former [147]. It has been demonstrated that when calculating the seismic response of the roof alone, compared to considering the entire large-span space structure with the lower structure in modal analysis, there are distinct differences in the frequencies of the first 10 orders. Simultaneously, nodal accelerations, roof displacements, and internal forces of rods show visible elevations [148]. This indicates that relying solely on the analysis of roofs is unreliable. Existing specifications [36] advocate for the co-calculation of the steel roof and lower supporting structure, emphasizing the need for considering damping ratio values in seismic design for large-span spatial structures. It is important to note that these recommended values were provided without taking into account the influence of different lower support structures and SSI effects.

Simultaneously, in the case of multi-degree-of-freedom (MDOF) structures, every mode contributes to the overall seismic response [149]. In the time history analysis of long-span structures, the most commonly employed method is the mode superposition method, where the key lies in determining the dominant modes [150]. Feng et al. [151] proposed the adoption of the mode contribution ratio to identify the dominant modes of spatial structures under seismic loads, a method that demonstrates greater precision compared to selecting the first 25~30 modes or using the effective mass method. The mentioned studies on SSI make it abundantly clear that SSI influences the modes of the structure, especially when the foundation type is a pile foundation or pile-raft foundation. Consequently, the higher-order modes of the structure exhibit more variation in the presence of SSI, underscoring the significance of considering the soil effects when conducting design or research.

Another crucial aspect of seismic investigation in the realm of large-span spatial structures is the consideration of multidimensional, multipoint, and nonstationary excitation. Typically, seismic response analysis of structures relies on the assumption of uniform excitation, utilizing the consistent input of ground motion. This approach predominantly considers the temporal variability of ground motion while omitting its spatial variation. However, the influence of Multiple Support Excitation (MSE) has garnered increased attention as the structural span expands [152]. Neglecting MSE could potentially lead to seismic design flaws [153]. Although early seismic response studies by Su and Dong [154] on a single-layer latticed shell with a diameter of 100 m suggested that the torsional effect induced by the travelling wave effect of vertical earthquakes could be mitigated by the substantial safety reserve in rods during actual engineering, subsequent seismic response studies on long-span structures and cable structures have revealed the inevitability of spatial variability [41,154]. This variability, observed in existing engineering practices [155–161], can either be amplified or discounted.

Since 2009, the authors' research group has been diligently addressing gaps in our understanding of the seismic response of SSI for large-span spatial structures. This subsection provides an overview of the ongoing work, along with a summary of the corresponding achievements. Utilizing advanced pile-soil models originally tailored for nuclear power plants and high-rise buildings, Luan [12] introduced a three-dimensional uncoupled pile-soil interaction model. This model incorporates the dynamic characteristics of spatial lattice structures subjected to strong seismic effects. Its feasibility was substantiated through a thorough comparison with a fully coupled analysis model. The initial assessment of the SSI effect was conducted using this model in the context of plane truss structures. The assumption of a single-layer site was in accordance with the U.S. code. The results indicated that the seismic responses of the structure on site Class E were notable when compared to those on site Class B, C, and D, and the SSI effect could be ignored. Sun [13] defined the relative stiffness β_1 between the supporting columns and upper roof, and took the site categorization of Chinese code as the soil condition to calculate the β_1 limit value of truss structures constructed on various sites, which ought to incorporate the SSI.

While measuring the structural self-resonance frequency of truss structures erected on site Class I, II, and III, the SSI effect had to be taken into consideration when $\beta_1 > 3$, and if evaluating the internal force response of the members, it had to be involved when $\beta_1 > 6$. For Class I and Class II sites, the SSI effect was hard to disregard when $\beta_1 > 1$, while for Class III sites, the limit value of β_1 was 6 for the numerical calculation of top chord nodes' acceleration. Since then, this pile–soil model has been applied to reticulated shell structures, where the displacements at the top of structures increased with decreasing soil stiffness when the superstructures remained unaltered, although the maximum bending moment of the main ribs might decrease. Similarly, Sun [13] determined the limit value of β_1 that had to be contemplated in terms of the SSI effect utilizing a double-layer Kiewitt dome reticulated shell structure with a span of 60 m as an example. The double-layer shell structure established on site Class II and III had β_1 limits of 0.6 and 0.1, each, whereas the SSI effect was negligible for the structure on site Class I when calculating the internal force of members. Parallel to such, while computing the effect of seismic acceleration of the mesh shells, the structure erected on site Class I could neglect the SSI effect as well. The β_1 limitations for structures built on site Class II and III were 0.2 and 0.1, respectively. Note that the site Class I₀, Class I₁, Class II, and Class III of Chinese code are equivalent to the site Class A, Class B, Class C (D), and Class D of the U.S. code, respectively.

It was demonstrated that the SSI effect played a favorable role in increasing overall damping and extending the structural period. Considering the relatively dense natural frequency of large-span spatial structures, the impact on vibration modes within the reticulated shell structure exceeded that in the truss structure, notably concentrated in the first five orders. Regardless of the SSI effect or the assumption of a rigid foundation, Wang [14] emphasized that the initial vibration mode of a reticulated shell structure tended to be horizontal due to its arched configuration, resulting in increased vertical stiffness and decreased horizontal stiffness. However, the SSI effect expedited the emergence of the vertical vibration mode, particularly manifesting sooner when the soil stiffness was lower. In models with a stiff or rigid base, the vertical vibration mode typically appeared in the 11th order; for medium-soft soil, it was in the 7th order; and for soft soil, it was in the 5th order.

Wang [14] and Wei [15] examined the dynamic stability of single-layer and double-layer reticulated shell structures under step loads, simple harmonic loads, and seismic waves, respectively, aiming to broaden the awareness of the dynamic characteristics of mesh shell structures whilst including SSI. For the single-layer reticulated shell structures, the incorporation of SSI could significantly reduce the seismic responses in terms of both the step and seismic loads, with the reduction ratio exceeding 20%. In other words, the assumption of a rigid foundation fundamentally enhanced the dynamic stability of the superstructure. Concerning simple harmonic loads as the input, the primary determining factor was whether the load frequency fell within the resonance range. The dynamic critical load of the structure was found to be less dependent on whether the SSI effect was considered or not. Additionally, analyzing attentively how the shell structure performed under various seismic effects and on different types of sites, it was discovered that, generally, the structural dynamic instability load tended to show lower values with the smaller the soil stiffness. Yet, the dynamic response of the shell under different sites and seismic waves varied significantly, and this tendency was not strictly linear and had a greater relationship with choices of seismic waves. Moreover, the failure mechanism was connected to the member section and the rise–span ratio. The structure was prone to strength fracture when the member section was smaller, and, in the opposite scenario, the structure was susceptible to buckling failure. Although the site influences the structural failure mechanism, it did not play an irreplaceable role. Wei [15] came to a similar conclusion for their research on the double-layer reticulated shell structure. Involving SSI resulted in a 10% increase in acceleration at the structural apex but a decrease in the lateral displacement. Furthermore, by applying sinusoidal loading, it was found that the plastic ratio of members, the maximum displacement of the structure, and the torsion angle were all amplified collectively

when the first period of structural self-resonance and the first-order self-resonance period of the soil coincide. Furthermore, for the sites with different periods, consideration ought to be given as well to the impact of the higher-order vibration mode on the structural response of shells. While the distribution of members' plasticity had been estimated, the area where the maximum displacement appeared differed significantly between the two cases of the structure without and with consideration for the SSI. It indicated that, even though the weak point remained virtually unaltered, the implications of the higher-order vibration modes on the structural impact were unavoidable after adopting SSI. A simplified simulation of SSI was established from Chinese code to attempt to explore the failure mechanism of the double-layer reticulated shell structure under the SSI effect, which contained the sites of Class I0, I1, II, III, and IV, respectively, and concluded that, for structures built on soft ground, extending the period of the structure may approximate the superior period of the input ground vibration, expanding the structural inertia during an earthquake and aggravating its hazard. Furthermore, an analysis based on numerical simulations of existing seismic design provisions indicates that the current seismic codes are suitable for high-rise buildings but may not apply to large-span structures. Instead, the torsional increase coefficients induced by SSI should be carefully considered when identifying the critical nodes in large-span spatial structures. Additionally, a pragmatic reference method for accurately evaluating the seismic performance of double-layer spherical reticulated shell structures was introduced in the form of a failure criterion.

A modified S–R (Sway–Rocking) model was offered by Wang [17] and Liu [16] based on the analysis of previous pile–soil simplified models by this group for the embedded method, the “m” method [162], and the resistance function method. The conclusion was that the resistance function is more accurate compared with other simplified methods for group pile foundations used for large-span spatial structures [12]. Shaking table tests were performed to confirm that the modified model had a better match with the assumed soil field, as illustrated in Figure 19. Liu [16] examined the seismic response of a single-layer cylindrical reticulated shell with various seismic wave incidence angles, foundation types (pile and independent foundations), and the presence or absence of seismic isolation bearings with the modified model, as illustrated in Figures 20–22. He also used shaking table tests to verify the results of the numerical simulation. The outcomes were consistent with our research group's earlier findings, which demonstrated that the SSI effect prolonged the structural period and elevated free-field acceleration by 5% to 30% at the foundation bottom and the soil surface. Simulated evaluation additionally proved that the incident angle profoundly impacted the seismic response of the structure. For example, in the case of P-wave incidence, maximum acceleration in both horizontal and vertical directions could be input proportionately to the ratio of 1:0.65 recommended by the *Code for the seismic design of buildings* [36] when the incidence angle was between 50° and 80°. However, when the incidence angle was between 0° and 50° and between 80° and 90°, the spatial effect of the seismic wave incidence required to be considered was increased. For the S-wave, the seismic response appeared to be enhanced when the input angle ranged between 30° and 60°. The ratio of the peak acceleration in the two horizontal directions at the base of the column fell between 1:0.3 and 1.3. As the intensity of the input seismic wave grew, the mutual coupling between the two horizontals was strengthened and the ratio approached 1:0.85. This range was further narrowed though, when seismic isolation bearings were applied, and, for S-waves, the interval to be pondered was 45°~60°. Based on the S–R modified model, Wang [17] carried out an initial investigation of the seismic response of a suspended dome structure with independent foundations. When the soil was considered, the structural frequency fluctuated similarly to that of the reticulated frames and shells, but its members' and nodes' acceleration responses deviated. The upper reticulated shell node's three displacements increased significantly after the SSI effect was considered, and, with softer soil, the displacements were larger, despite changes being unnoticeable. Meanwhile, the three accelerations of nodes dropped considerably, and the acceleration gradually decreased with the soil stiffness reduced. Meanwhile, the maximum compressive stresses

of the braces, the maximum tensile stresses of the diagonal members and ring cables, and the initial prestress loss of the ring cables all significantly decreased at the same time as the maximum compressive stresses of the ring and radial members of the reticulated shell increased.

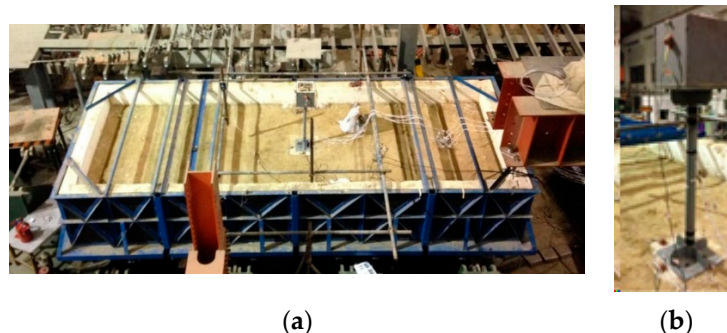


Figure 19. Shaking table test of single-column mass structure–soil interaction [17]: (a) soil container with experimental model; (b) single-column mass structure.

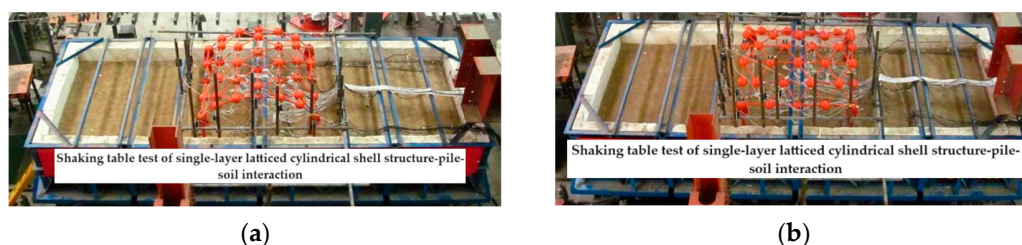


Figure 20. Shaking table test of single-layer latticed cylindrical shell structure–pile–soil interaction under vertical incidence of seismic waves [16]: (a) vertical arrangement; (b) parallel arrangement.



Figure 21. Shaking table test of single-layer latticed cylindrical shell structure–independent foundation–soil interaction under vertical and oblique incidence of seismic waves [16]: (a) vertical arrangement; (b) parallel arrangement.



Figure 22. Shaking table test of single-layer latticed cylindrical shell structure-independent foundation–soil interaction considering seismic isolation [16]: (a) soil container with experimental model; (b) layered rubber bearing and its connection.

The author's group is presently engaged in evaluating the SSI effect on suspended dome structures at actual sites, aiming to provide a deeper understanding of the seismic response of prestressed structures. The Chinese code is adopted as a basis for site classification and wave selection to analyze the effects of SSI on the dynamic response of the structure and provide an approximate spectrum of impact. The superstructure depends on an actual construction, the Lanzhou Olympic Sports Center, as illustrated in Figure 23. Earlier studies primarily focused on a simplified model employing a continuous spring unit to replicate the influence of soil on the structure. The soil model was derived from a hypothetical site and lacked refinement, potentially leading to a scenario where the seismic response of the structure deviated from the actual seismic conditions. The two subclasses I0 and I1 of the site Class I, which have a large stiffness and approximate rigid foundation assumption, are not included in the current research scope. Existing results indicate that the sites that need to take the SSI into account primarily are sites Class II, III, and IV. To generate more reliable FEM, the soil models for site Class II, III, and IV in the ongoing study rely on real locations. Seismic waves are selected using two methods: employing standard response spectra and utilizing seismic waves that were measured at the modelled site. It is anticipated that these improvements will enhance the credibility of structural seismic responses at the site, providing empirical coefficients for the SSI effect. These coefficients can be utilized in subsequent endeavors, particularly in the investigations of prestressed structures.

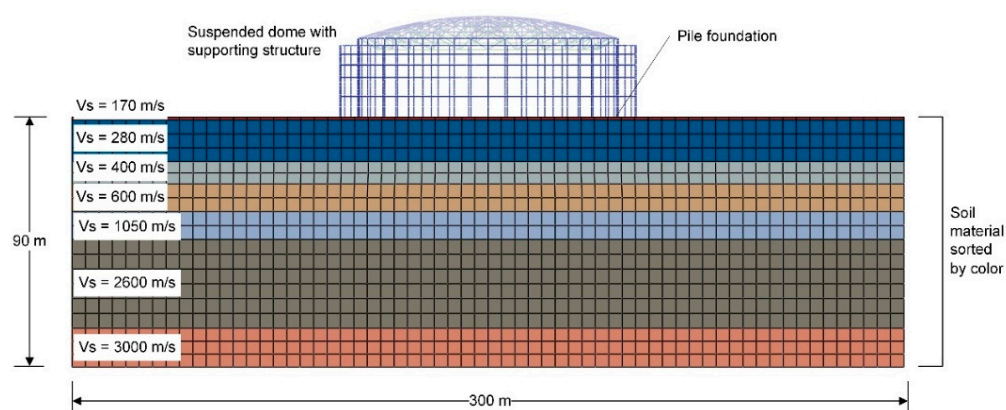


Figure 23. Model of Lanzhou Olympic Sports Center considering SSI.

6. Conclusions and Future Research Directions

In this paper, Section 2 elucidated prevalent solutions for SSI effects, while Sections 3 and 4 comprehensively reviewed site conditions, seismic excitation, the foundation type, and superstructure arrangement's impact on the seismic response of the entire system. These discussions were conducted under the two main categories of numerical and experimental studies for general structures. Section 5 delved into the significance of considering SSI for large-span spatial structures, providing an updated overview of the state of research on SSI effects in this context. In conclusion, this section will summarize key insights drawn from prior investigations and propose research directions for SSI systems involving large-span spatial structures.

6.1. Synthesis of Research Conclusions

(1) Chinese Codes mandate the consideration of the SSI effect for site Class II, III, and IV. For site Class I, SSI can be neglected in the absence of particular topographic conditions, as confirmed by studies on frame structures. However, for specific types of space structures erected on site Class I, the SSI effect cannot be dismissed when the stiffness ratio of the supporting structure to the upper roof surpasses a specified limit. Additionally, it is imperative to account for the thickness and burial depth of the weak layer, as these factors play decisive roles in influencing seismic wave effects.

(2) While the soil effect generally dominates in most scenarios, it is crucial to note that this is not universally applicable. The impact of a slope on the SSI system is largely contingent on the ratio of the distance between the structure and the slope to the height of the slope. Although values across different papers may vary, there is a common agreement that the slope effect can be disregarded when the ratio exceeds 5. However, a consensus is yet to be reached on the specific amplification factor of the slope effect, and this necessitates examination in light of the specific characteristics of the site.

(3) According to the response spectrum, seismic waves could be selected to reduce the calculation error. Furthermore, a distinct spatial effect is observed, indicating that the seismic responses of structures do not increase linearly with various incidence angles. The determination of the most unfavorable incidence angle under three-dimensional seismic wave input is structure and site-dependent.

(4) Foundations exhibit diverse responses to SSI, with shallow and compensatory foundations being more susceptible compared to pile and pile–raft foundations. Additionally, the SSI effect has the potential to alleviate the base shear force, with pile and pile–raft foundations demonstrating higher discount factors than shallow foundations.

(5) In the case of frame structures, SSI may lead to a reduction in low-order modal frequency and an extension of the structural period. However, owing to their unique structural characteristics, large-span spatial structures should also consider the effects of SSI on high-order modes. Additionally, prior research has established that different superstructures exhibit varying degrees of sensitivity to SSI effects, primarily manifested in the increase or decrease in peak horizontal acceleration, inter-story drift ratio, and lateral displacement of the structure.

(6) Incorporating the nonlinear properties of soil becomes imperative when dealing with long site periods, as the application of a linear soil model introduces greater errors with increasing site periods. The direct method, devoid of the need for the superposition of multiple simplifying assumptions, allows for accurate nonlinear analysis of the SSI system, maintaining optimal accuracy. Unfortunately, its extensive computational demands render it impractical for use in large-scale models within engineering practice.

6.2. Prospective Research Directions

In light of the aforementioned considerations regarding the importance of integrating SSI in the design of large-span spatial structures, and acknowledging the ongoing debate on the applicability of existing research findings from other structures to the study of space structures, coupled with the recognized need for additional numerical and experimental simulations, this section will delve into potential future research directions for large-span spatial structures considering SSI. These directions are based on insights gleaned from previous investigations on other structure types, as well as the ongoing and completed research within the authors' research group.

(1) A more comprehensive and in-depth experimental or theoretical study would be beneficial to explore this aspect of the influence coefficient. *Code for seismic design of buildings* [36] stipulates that, for buildings constructed on sites Class III and IV, when SSI are included, the horizontal seismic shear tends to be diminished. Nonetheless, the group's research [14–17] revealed that, in certain circumstances, the horizontal seismic response was heightened rather than discounted, attributed to the influence of the higher-order vibration modes.

(2) Different numerical simulations have implemented various hypotheses and degrees of simplifying as dynamic interaction spans a wide range of research areas. Hence, the structural and foundation responses offered through several computational models might vary greatly from one another. Most SSI effects generated from two-dimensional modeling, such as dams or frame structures, may not be appropriate for spatial structures since their seismic vibrations are three-dimensional [163]. Meanwhile, there are a variety of spatial structures, along with numerous influencing factors. Certain large projected scale spatial structures ($span \geq 120$ m, $length \geq 300$ m, $cantilever \geq 40$ m) are obliged to

contain multidirectional and multipoint inputs, which involve seismic wave reflection and diffraction. Thus, a more systematic study is necessary for various structural forms.

(3) It is imperative to recognize that diverse subsurface structures influence SSI. Recent articles often employ high-rise buildings and bridges as superstructures to investigate the impact of underground foundation design on the seismic response of SSI systems, with a significant focus on pile foundations and pile–raft foundations. However, the seismic assessment of large-span constructions with different foundation types, particularly in the context of larger underground spaces, is not thoroughly explored. It is advisable to delve deeper, as the presence of a basement imposes greater constraints on the superstructure compared to pile foundations.

(4) Studies conducted thus far on SSI in large-span structures commonly overlook scenarios in which both the superstructure and the soil simultaneously undergo plasticity. The equivalent strain of the soil experiences significant development during rare earthquakes, particularly in sites with soft soil layers, while certain members of the superstructure gradually enter plasticity. To accurately simulate the outcomes of seismic responses and determine whether structures eventually face dynamic instability, strength damage, or support failure, it is crucial to incorporate more sophisticated nonlinear or equivalent linear soil models and robust superstructure models that consider the plastic damage of materials in similar situations.

(5) There remains a discrepancy between experimental results and real ground vibrations, primarily attributed to the predominantly small-scale nature of previous experimental studies on SSI. A critical aspect of this process involves the selection of laboratory soil material. Using genuine soil introduces significant challenges; accurately scaling density and particle size, rearranging internal filler during vibration, and addressing other complexities pose inherent difficulties [145]. Alternatively, using a substitute would hinder the accurate simulation of soil nonlinearity. Furthermore, research on the topographic effects is confined by the limitations of the test site. The author's group conducted a comprehensive examination of the spatial effects of a single cylindrical reticulated shell under oblique incidence of seismic waves through numerical analysis and experiments. [16] Unfortunately, due to the model spans of the sizes of test models being relatively small, the travelling wave effect was not further involved. Furthermore, to ensure the generalizability of test results for practical engineering applications, larger-scale shaking table tests or field testing may be necessary, especially for broader spans.

(6) Further, as highlighted in this introduction, mitigating the impact of SSI is impractical when assessing the vibration control for large-span spatial structures. The vibration-damping effectiveness of the tuned mass damper (TMD) system, founded on the assumption of a rigid foundation, may prove suboptimal on flexible foundations and could potentially yield adverse effects, as evidenced by tests. Hence, further investigations are imperative to scrutinize the influence of SSI, validate their feasibility, and assess their damping effects.

Author Contributions: Conceptualization, X.L. and G.S.; validation, S.X.; writing—original draft preparation, P.Z.; writing—review and editing, P.Z. and R.M.; funding acquisition, X.L. All authors have read and agreed to the published version of the manuscript.

Funding: This research was funded by the National Key Research and Development Program of China (No. 2023YFC3805603).

Data Availability Statement: Not applicable.

Conflicts of Interest: The authors declare no conflicts of interest.

References

1. Kausel, E. Early history of soil-structure interaction. *Soil Dyn. Earthq. Eng.* **2010**, *30*, 822–832. [[CrossRef](#)]
2. Wu, S.; Gan, G. Dynamic soil-structure interaction for high-rise buildings. *Dev. Geotech. Eng.* **1998**, *83*, 203–216. [[CrossRef](#)]
3. Xia, D.; He, Y.; Liu, J. Study of damping property and seismic action effect for soil-structure dynamic interaction system. *Rock Soil Mech.* **2009**, *30*, 2923–2928. (In Chinese) [[CrossRef](#)]

4. FEMA 440; Improvement of Nonlinear static Seismic Analysis Procedures. Applied Technology Council (ATC): Redwood City, CA, USA, 2005.
5. Lou, M.; Wang, H.; Chen, X.; Zhai, Y. Structure-soil-structure interaction: Literature review. *Soil Dyn. Earthq. Eng.* **2011**, *31*, 1724–1731. [[CrossRef](#)]
6. Wang, H.; Lou, M.; Chen, X.; Zhai, Y. Structure-soil-structure interaction between underground structure and ground structure. *Soil Dyn. Earthq. Eng.* **2013**, *54*, 31–38. [[CrossRef](#)]
7. Abdulaziz, M.A.; Hamood, M.J.; Fattah, M.Y. A review study on Seismic behavior of individual and adjacent structures considering the soil-Structure interaction. *Structures* **2023**, *52*, 348–369. [[CrossRef](#)]
8. Naji, M.; Firoozi, A.A.; Firoozi, A.A. A review: Study of integral abutment bridge with consideration of soil-structure interaction. *Lat. Am. J. Solids Struct.* **2020**, *17*, e252. [[CrossRef](#)]
9. Jeremić, B.; Jie, G.; Preisig, M.; Tafazzoli, N. Time domain simulation of soil-foundation-structure interaction in non-uniform soils. *Earthq. Eng. Struct. Dyn.* **2009**, *38*, 699–718. [[CrossRef](#)]
10. Taslimi, A.; Petrone, F.; Pitarka, A. Characteristics of vertical ground motions and their effect on the seismic response of bridges in the near-field: A state-of-the-art review. *J. Bridge Eng.* **2024**, *29*, 03124001. [[CrossRef](#)]
11. Sigdel, L.D.; Al-Qarawi, A.; Leo, C.J.; Liyanapathirana, S.; Hu, P. Geotechnical design practices and soil-structure interaction effects of an integral bridge system: A review. *Appl. Sci.* **2021**, *11*, 7131. [[CrossRef](#)]
12. Xue, S.; Luan, X.; Li, X. Effect of soil conditions on the seismic response of spatial structure. *Adv. Mater. Res.* **2011**, 368–373, 2079–2083. [[CrossRef](#)]
13. Sun, Y. Dynamical Performance Analysis of Space Lattice Structure Considering Soil-Foundation-Structure Interaction. Master's Dissertation, Beijing University of Technology, Beijing, China, 2010. (In Chinese)
14. Wang, G. Study on Dynamic Stability of Single-Layer Reticulated Domes Considering Soil-Structure Interaction Subjected to Earthquake Motion. Master's Dissertation, Beijing University of Technology, Beijing, China, 2011. (In Chinese)
15. Wei, X. Failure Mechanism for Double-Layer Latticed Shells Considering Soil-Structure Interaction. Master's Dissertation, Beijing University of Technology, Beijing, China, 2011. (In Chinese)
16. Liu, Y. Seismic Analysis and Experimental Investigation for Soil-Lattice Structure Interaction System. Ph.D. Dissertation, Beijing University of Technology, Beijing, China, 2015. (In Chinese)
17. Wang, G. Numerical Simulation and Experimental Research of Simplified SSI Method of Modified S-R Model. Master's Dissertation, Beijing University of Technology, Beijing, China, 2015. (In Chinese)
18. GB 55003-2021; General Code for Foundation Engineering of Building and Municipal Projects. Ministry of Housing and Urban-Rural Development of the People's Republic of China (MOHURD): Beijing, China, 2021. (In Chinese)
19. Hokmabadi, A.S.; Fatahi, B. Influence of foundation type on seismic performance of buildings considering soil-structure interaction. *Int. J. Struct. Stab. Dyn.* **2016**, *16*, 1550043. [[CrossRef](#)]
20. Ghazavi, M.; Dehkordi, P.F. Interference influence on behavior of shallow footings constructed on soils, past studies to future forecast: A state-of-the-art review. *Transp. Geotech.* **2021**, *27*, 100502. [[CrossRef](#)]
21. Vergara, J.; Sierra, C.; Sáenz, M.; Jaramillo, J.; Gomez, J. Construction of rational models for topographic effects and size-conditioned-response-spectra. *Soil Dyn. Earthq. Eng.* **2021**, *140*, 106432. [[CrossRef](#)]
22. Houston, H.; Kanamori, H. Source characteristics of the 1985 Michoacan, Mexico Earth-quake at periods of 1 to 30 seconds. *Geophys. Res. Lett.* **1986**, *13*, 597–600. [[CrossRef](#)]
23. Chen, J.; Chen, X.; Shi, G. Research on seismic response characteristics of sites with deep and soft soils. *J. Disaster Prev. Mitig. Eng.* **2004**, *24*, 131–138, (In Chinese) [[CrossRef](#)]
24. Jin, D.; Chen, G.; Dong, F. Seismic response of a real basin site considering topography effect and nonlinear characteristic of soil. In Proceedings of the Sixth China-Japan-US Trilateral Symposium on Lifeline Earthquake Engineering, Chengdu, China, 28 May–1 June 2013; pp. 545–552. [[CrossRef](#)]
25. Zhao, C.; Valliappan, S. Incident P and SV wave scattering effects under different canyon topographic and geological conditions. *Int. J. Numer. Anal. Methods Geomech.* **1993**, *17*, 73–94. [[CrossRef](#)]
26. Zhao, C.; Valliappan, S. Seismic wave scattering effects under different canyon topographic and geological conditions. *Soil Dyn. Earthq. Eng.* **1993**, *12*, 129–143. [[CrossRef](#)]
27. Fatahi, B.; Huang, B.; Yeganeh, N.; Terzaghi, S.; Banerjee, S. Three-dimensional simulation of seismic slope-foundation-structure interaction for buildings near shallow slopes. *Int. J. Geomech.* **2020**, *20*, 04019140. [[CrossRef](#)]
28. Brennan, A.J.; Madabhushi, S.P.G. Amplification of seismic accelerations at slope crests. *Can. Geotech. J.* **2009**, *46*, 585–594. [[CrossRef](#)]
29. Alitalesh, M.; Shahnazari, H.; Baziar, M.H. Parametric study on seismic topography-soil-structure interaction; Topographic effect. *Geotech. Geol. Eng.* **2018**, *36*, 2649–2666. [[CrossRef](#)]
30. Raj, D.; Singh, Y.; Kaynia, A.M. Behavior of slopes under multiple adjacent footings and buildings. *Int. J. Geomech.* **2018**, *18*, 04018062. [[CrossRef](#)]
31. Madany, M.; Guo, P.J. Structure-soil-structure interaction analysis for lateral seismic earth pressure of deeply buried structure in layered ground. *Int. J. Geomechanics.* **2021**, *21*, 04021217. [[CrossRef](#)]
32. Clouteau, D.; Broc, D.; Devésá, G.; Guyonvarh, V.; Massin, P. Calculation methods of structure-soil-structure interaction (3SI) for embedded buildings: Application to NUPEC tests. *Soil Dyn. Earthq. Eng.* **2012**, *32*, 129–142. [[CrossRef](#)]

33. Far, H. Advanced computation methods for soil-structure interaction analysis of structures resting on soft soils. *Int. J. Geotech. Eng.* **2019**, *13*, 352–359. [[CrossRef](#)]
34. Idriss, I.M.; Seed, H.B. Seismic response of horizontal soil layers. *J. Soil Mech. Found. Div.* **1968**, *94*, 1003–1031. [[CrossRef](#)]
35. GB 17741-2005; Evaluation of Seismic Safety for Engineering Site. Standardization Administration of the People's Republic of China (SAC): Beijing, China, 2014. (In Chinese)
36. GB 50011-2010; Code for Seismic Design of Buildings. Ministry of Housing and Urban-Rural Development of the People's Republic of China (MOHURD): Beijing, China, 2016. (In Chinese)
37. Ni, S.; Li, S.; Chang, Z.; Xie, L. An alternative construction of normalized seismic design spectra for near-fault regions. *Earthq. Eng. Eng. Vib.* **2013**, *12*, 351–362. [[CrossRef](#)]
38. Rodriguez-Marek, A.; Song, J. Displacement-Based Probabilistic Seismic Demand Analyses of Earth Slopes in the Near-Fault Region. *Earthq. Spectra* **2016**, *32*, 1141–1163. [[CrossRef](#)]
39. Kiureghian, A.D. A coherency model for spatially varying ground motions. *Earthq. Eng. Struct. Dyn.* **1996**, *25*, 99–111. [[CrossRef](#)]
40. Harichandran, R.S.; Vanmarcke, E.H. Stochastic variation of earthquake ground motion in space and time. *J. Eng. Mechanics.* **1986**, *112*, 154–174. [[CrossRef](#)]
41. Wang, X.; Xue, S.; Cao, Z. Nonstationary response of spatial lattice shells under multiple seismic inputs. In Proceedings of the International Conference on Advances in Building Technology (ABT 2002), Hong Kong, 4–6 December 2002; pp. 595–602.
42. Jaya, K.P.; Prasad, A.M. Embedded foundation in layered soil under dynamic excitations. *Soil Dyn. Earthq. Eng.* **2002**, *22*, 485–498. [[CrossRef](#)]
43. Stewart, J.; Crouse, C.B.; Hutchinson, T.C.; Lizundia, B.; Naeim, F.; Ostadan, F. *Soil-Structure Interaction for Building Structures (NIST GCR 12-917-21)*; NIST Pubs: Gaithersburg, MD, USA, 2012.
44. Anoyatis, G.; Lemnitzer, A. Kinematic Winkler modulus for laterally-loaded piles. *Soils Found.* **2017**, *57*, 453–471. [[CrossRef](#)]
45. Dhadse, G.D.; Ramtekkar, G.D.; Bhatt, G. Finite element modeling of soil structure interaction system with interface: A review. *Arch. Comput. Methods Eng.* **2021**, *28*, 3415–3432. [[CrossRef](#)]
46. Jemielita, G. Governing equations and boundary conditions of a generalized model of elastic foundation. *J. Theor. Appl. Mech.* **1994**, *32*, 887–901.
47. Zhao, X.; Zhu, W.; Li, Y.; Li, M.; Li, X. Review, classification, and extension of classical soil-structure interaction models based on different superstructures and soils. *Thin-Walled Struct.* **2022**, *173*, 108936. [[CrossRef](#)]
48. Anand, V.; Kumar, S.R.S. Seismic soil-structure interaction: A state-of-the-art review. *Structures* **2018**, *16*, 317–326. [[CrossRef](#)]
49. Veletsos, A.S.; Tang, A.Y. Vertical vibration of ring foundations. *Earthq. Eng. Struct. Dyn.* **1987**, *15*, 1–21. [[CrossRef](#)]
50. Gazetas, G. Formulas and charts for impedances of surface and embedded foundations. *J. Geotech. Eng.* **1991**, *117*, 1363–1381. [[CrossRef](#)]
51. Chen, W. A dynamical nonlinear effective stress method to evaluate liquefaction of subsoil of building used cone model. *Rock Soil Mech.* **2003**, *24*, 40–44. (In Chinese) [[CrossRef](#)]
52. Dutta, S.C.; Roy, R. A critical review on idealization and modeling for interaction among soil-foundation-structure system. *Comput. Struct.* **2002**, *80*, 1579–1594. [[CrossRef](#)]
53. Wen, Y.; Yang, G.; Zhong, Z. Multipotential surface elastoplastic constitutive model and its application in the analysis of the phase II cofferdam of the three gorges project. *Geofluids* **2023**, *2023*, 9581827. [[CrossRef](#)]
54. Mott, G.; Wang, J. The effects of variable soil damping on soil-structure dynamics. *J. Vib. Control* **2011**, *17*, 365–371. [[CrossRef](#)]
55. Chen, W.F.; Saleeb, A.F. *Elasticity and Plasticity*; Yu, T., Wen, X., Liu, Z., Eds.; China Architecture & Building Press: Beijing, China, 2016.
56. Seed, H.B.; Idriss, I.M. *Soil Moduli and Damping Factors for Dynamic Response Analyses*; Technical Report; National Technical Reports Library: Lawrence, KS, USA, 1970. Available online: <https://ntrl.ntis.gov/NTRL/dashboard/searchResults/titleDetail/PB197869.xhtml> (accessed on 24 July 2023).
57. Bolisetti, C.; Whittaker, A.S.; Coleman, J.L. Linear and nonlinear soil-structure interaction analysis of buildings and safety-related nuclear structures. *Soil Dyn. Earthq. Eng.* **2018**, *107*, 218–233. [[CrossRef](#)]
58. Ghandil, M.; Behnamfar, F. The near-field method for dynamic analysis of structures on soft soils including inelastic soil-structure interaction. *Soil Dyn. Earthq. Eng.* **2015**, *75*, 1–17. [[CrossRef](#)]
59. Deng, H.; Jin, X.; Gu, M.; Huang, J. Modification of soil dynamic constitutive model in pile-soil-structure interaction analysis. *J. Tongji Univ. (Nat. Sci.)* **2018**, *46*, 1473–1478+1574. (In Chinese) [[CrossRef](#)]
60. Masing, G. Eigenspannungen und verfestigung beim messung. In Proceedings of the Second International Congress of Applied Mechanics, Zurich, Switzerland, 12–17 September 1926; pp. 332–335.
61. Hardin, B.O.; Drnevich, V.P. Shear modulus and damping in soils: Design equations and curves. *J. Soil Mech. Found. Div.* **1972**, *98*, 667–692. [[CrossRef](#)]
62. Kim, D.S.; Stokoe, K.H. Soil damping computed with Ramberg-Osgood-Masing model. In Proceedings of the 13th International Conference on Soil Mechanics and Foundation Engineering, New Delhi, India, 5–10 January 1994; pp. 211–214.
63. Martin, P.P.; Seed, H.B. *A Computer Program for the Non-Linear Analysis of Vertically Propagating Shear Waves in Horizontally Layered Deposits*; Technical Report; Earthquake Engineering Research Center: Oakland, CA, USA, 1978.
64. Martin, P.P.; Seed, H.B. One-dimensional dynamic ground response analyses. *J. Geotech. Eng. Div.* **1982**, *108*, 935–952. [[CrossRef](#)]
65. Pyke, R.M. Nonlinear soil models for irregular cyclic loadings. *J. Geotech. Eng. Div.* **1980**, *106*, 1281–1282. [[CrossRef](#)]

66. Liu, J.; Gu, Y.; Du, Y. Consistent viscous-spring artificial boundaries and viscous-spring boundary elements. *Chin. J. Geotech. Eng.* **2006**, *28*, 1070–1075. (In Chinese)
67. Song, E.; Luo, S. A local artificial boundary for transient seepage problems with unsteady boundary conditions in unbounded domains. *Int. J. Numer. Anal. Methods Geomech.* **2017**, *41*, 1108–1124. [[CrossRef](#)]
68. Bettess, P. Infinite elements. *Int. J. Numer. Methods Eng.* **1977**, *11*, 53–64. [[CrossRef](#)]
69. Lysmer, J.; Kuhlemeyer, R.L. Finite dynamic model for infinite media. *J. Eng. Mech. Div.* **1969**, *95*, 859–877. [[CrossRef](#)]
70. Zhang, G.; Zhao, M.; Wang, P.; Du, X.; Zhang, X. Obliquely incident P-SV wave scattering by multiple structures in layered half space using combined zigzag-paraxial boundary condition. *Soil Dyn. Earthq. Eng.* **2021**, *143*, 106662. [[CrossRef](#)]
71. Chang, X.; Liu, D.; Gao, F.; Lu, L.; Long, L.; Zhang, J.; Geng, X. A study on lateral transient vibration of large diameter piles considering pile-soil interaction. *Soil Dyn. Earthq. Eng.* **2016**, *90*, 211–220. [[CrossRef](#)]
72. Bazyar, M.H.; Song, C. A continued-fraction-based high-order transmitting boundary for wave propagation in unbounded domains of arbitrary geometry. *Int. J. Numer. Methods Eng.* **2008**, *74*, 209–237. [[CrossRef](#)]
73. Chen, S.S.; Hsu, W.C. An energy transmitting boundary for semi-infinite structures. *J. Mech.* **2007**, *23*, 159–172. [[CrossRef](#)]
74. Liu, T.; Zheng, S.; Tang, X.; Gao, Y. Time-Domain Analysis of Underground Station-Layered Soil Interaction Based on High-Order Doubly Asymptotic Transmitting Boundary. *Comput. Model. Eng. Sci.* **2019**, *120*, 545–560. [[CrossRef](#)]
75. Gu, Y.; Bo, J.; Du, Y. 3D consistent viscous-spring artificial boundary and viscous-spring boundary element. *Eng. Mech.* **2007**, *24*, 31–37. (In Chinese)
76. Liu, J.; Li, B. Three-dimensional viscoelastic static and dynamic unified artificial boundary. *Sci. Sin. (Technol.)* **2005**, *9*, 72–86. (In Chinese)
77. Semblat, J.F. Modeling seismic wave propagation and amplification in 1D/2D/3D linear and nonlinear unbounded media. *Int. J. Geomech.* **2011**, *11*, 440–448. [[CrossRef](#)]
78. Tsai, H.C. Modal superposition method for dynamic analysis of structures excited by prescribed support displacements. *Comput. Struct.* **1998**, *66*, 675–683. [[CrossRef](#)]
79. Tian, Y.; Yang, Q. On time-step in structural seismic response analysis under ground displacement/acceleration. *Earthq. Eng. Eng. Vib.* **2009**, *8*, 341–347. [[CrossRef](#)]
80. Liu, J.; Dong, Y. A direct method for analysis of dynamic soil-structure interaction. *China Civ. Eng. J.* **1998**, *31*, 55–64. (In Chinese) [[CrossRef](#)]
81. Liu, J.; Bao, X.; Wang, D. The internal substructure method for seismic wave input in 3D dynamic soil-structure interaction analysis. *Soil Dyn. Earthq. Eng.* **2019**, *127*, 105847. [[CrossRef](#)]
82. He, J.; Ma, H.; Zhang, B.; Chen, H. Method and realization of seismic motion input of viscous-spring boundary. *J. Hydraul. Eng.* **2010**, *41*, 960–969. (In Chinese) [[CrossRef](#)]
83. Kim, M.K.; Lim, Y.M.; Cho, W.Y. Three dimensional dynamic response of surface foundation on layered half-space. *Eng. Struct.* **2001**, *23*, 1427–1436. [[CrossRef](#)]
84. Liu, J.; Wang, Y. A 1D time-domain method for in-plane wave motions in a layered half-space. *Acta Mech. Sin.* **2007**, *23*, 673–680. [[CrossRef](#)]
85. Zhang, J.; Li, M.; Han, S. Seismic analysis of gravity dam-layered foundation system subjected to earthquakes with arbitrary incident angles. *Int. J. Geomech.* **2022**, *22*, 04021279. [[CrossRef](#)]
86. Liu, J.; Tan, H.; Bao, X.; Wang, D.; Li, S. Seismic wave input method for three-dimensional soil-structure dynamic interaction analysis based on the substructure of artificial boundaries. *Earthq. Eng. Eng. Vib.* **2019**, *18*, 747–758. [[CrossRef](#)]
87. Saberi, M.; Annan, C.D.; Konrad, J.M. On the mechanics and modeling of interfaces between granular soils and structural materials. *Arch. Civ. Mech. Eng.* **2018**, *18*, 1562–1579. [[CrossRef](#)]
88. Uesugi, M.; Kishida, H. Frictional resistance at yield between dry sand and mild steel. *Soils Found.* **1986**, *26*, 139–149. [[CrossRef](#)]
89. Zhang, G.; Zhang, J. State of the art: Mechanical behavior of soil-structure interface. *Prog. Nat. Sci.* **2009**, *19*, 1187–1196. [[CrossRef](#)]
90. Ma, J.; Wang, D.; Randolph, M.F. A new contact algorithm in the material point method for geotechnical simulations. *Int. J. Numer. Anal. Methods Geomech.* **2014**, *38*, 1197–1210. [[CrossRef](#)]
91. Clough, G.W.; Duncan, J.M. Finite element analyses of retaining wall behavior. *J. Soil Mech. Found. Div.* **1971**, *97*, 1657–1673. [[CrossRef](#)]
92. Desai, C.S.; Zaman, M.M.; Lightner, J.G.; Siriwardane, H.J. Thin-layer element for interfaces and joints. *Int. J. Numer. Anal. Methods Geomech.* **1984**, *8*, 19–43. [[CrossRef](#)]
93. Genes, M.C.; Kocak, S. Dynamic soil-structure interaction analysis of layered unbounded media via a coupled finite element/boundary element/scaled boundary finite element model. *Int. J. Numer. Methods Eng.* **2005**, *62*, 798–823. [[CrossRef](#)]
94. Padrón, L.A.; Aznárez, J.J.; Maeso, O. 3-D boundary element-finite element method for the dynamic analysis of piled buildings. *Eng. Anal. Bound. Elem.* **2011**, *35*, 465–477. [[CrossRef](#)]
95. Shehata, O.E.; Farid, A.F.; Rashed, Y.F. Practical boundary element method for piled rafts. *Eng. Anal. Bound. Elem.* **2018**, *97*, 67–81. [[CrossRef](#)]
96. Wolf, J.P. Response of unbounded soil in scaled boundary finite-element method. *Earthq. Eng. Struct. Dyn.* **2002**, *31*, 15–32. [[CrossRef](#)]
97. Tadeu, A.J.B.; Kausel, E.; Vrettos, C. Scattering of waves by subterranean structures via the boundary element method. *Soil Dyn. Earthq. Eng.* **1996**, *15*, 387–397. [[CrossRef](#)]

98. Mohammadi, M.; Karabalis, D.L. Dynamic 3-D soil-railway track interaction by BEM-FEM. *Earthq. Eng. Struct. Dyn.* **1995**, *24*, 1177–1193. [[CrossRef](#)]
99. Yazdchi, M.; Khalili, N.; Valliappan, S. Dynamic soil-structure interaction analysis via coupled finite-element-boundary-element method. *Soil Dyn. Earthq. Eng.* **1999**, *18*, 499–517. [[CrossRef](#)]
100. Chen, X.; Birk, C.; Song, C. Numerical modelling of wave propagation in anisotropic soil using a displacement unit-impulse-response-based formulation of the scaled boundary finite element method. *Soil Dyn. Earthq. Eng.* **2014**, *65*, 243–255. [[CrossRef](#)]
101. Lu, S.; Liu, J.; Lin, G. Hamiltonian-based derivation of the high-performance scaled-boundary finite-element method applied to the complex multilayered soil field in time domain. *Int. J. Geomech.* **2016**, *16*, 04015098. [[CrossRef](#)]
102. Hassanen, M.; El-Hamalawi, A. Two-dimensional development of the dynamic coupled con-solidatio5 scaled boundary finite-element method for fully saturated soils. *Soil Dyn. Earthq. Eng.* **2007**, *27*, 153–165. [[CrossRef](#)]
103. Birk, C.; Behnke, R. A modified scaled boundary finite element method for three-dimensional dynamic soil-structure interaction in layered soil. *Int. J. Numer. Methods Eng.* **2012**, *89*, 371–402. [[CrossRef](#)]
104. Liang, J.; Wu, M.; Ba, Z.; Lee, V.W. Surface motion of a layered transversely isotropic half-space with a 3D arbitrary-shaped alluvial valley under qP-, qSV- and SH-waves. *Soil Dyn. Earthq. Eng.* **2021**, *140*, 106388. [[CrossRef](#)]
105. Tripe, R.; Kontoe, S.; Wong, T.K.C. Slope topography effects on ground motion in the presence of deep soil layers. *Soil Dyn. Earthq. Eng.* **2013**, *50*, 72–84. [[CrossRef](#)]
106. Vicencio, F.; Alexander, N.A. Dynamic interaction between adjacent buildings through non-linear soil during earthquakes. *Soil Dyn. Earthq. Eng.* **2018**, *108*, 130–141. [[CrossRef](#)]
107. Lan, J.; Liu, J.; Song, X. Study on the influence of the seafloor soft soil layer on seismic ground motion. *Nat. Hazards Earth Syst. Sci.* **2021**, *21*, 577–585. [[CrossRef](#)]
108. Chen, S.; Zhu, X.; Zhao, Y.; Chen, G. Analysis of saturated soil-structure interaction considering soil skeleton nonlinearity. *Earthq. Eng. Eng. Dyn.* **2019**, *39*, 114–127. (In Chinese) [[CrossRef](#)]
109. Ding, Y.; Pagliaroli, A.; Lanzo, G. One-dimensional seismic response of two-layer soil deposits with shear wave velocity inversion. In Proceedings of the AIP 2008 Seismic Engineering Conference: Commemorating the 1908 Messina and Reggio Calabria Earth-quake Reggio Calabria, Reggio Calabria, Italy, 8–11 July 2008; Volume 1020, pp. 252–258. [[CrossRef](#)]
110. Iida, M. 3D methods for examining soil-building interaction for nonlinear soil behavior based on an input wave field. *Int. J. Geomech.* **2017**, *17*, 04016081. [[CrossRef](#)]
111. Iida, M. Three-dimensional nonlinear soil response methods based on a three-component input wave field. *Int. J. Geomech.* **2016**, *16*, 04015026. [[CrossRef](#)]
112. Shahbazi, M.; Cerato, A.B.; El Naggar, M.H.; Elgamel, A. Evaluation of seismic soil-structure interaction of full-scale grouped helical piles in dense sand. *Int. J. Geomech.* **2020**, *20*, 04020228. [[CrossRef](#)]
113. Xu, R.; Fatahi, B.; Hokmabadi, A.S. Influence of soft soil shear strength on the seismic response of concrete buildings considering soil-structure interaction. In Proceedings of the Advances in Numerical and Experimental Analysis of Transportation Geomaterials and Geosystems for Sustainable Infrastructure (Geo-China 2016), Shandong, China, 25–27 July 2016; pp. 17–24. [[CrossRef](#)]
114. Mercado, J.A.; Mackie, K.R.; Arboleda-Monsalve, L.G. Modeling nonlinear-inelastic seismic response of tall buildings with soil-structure interaction. *J. Struct. Eng.* **2021**, *147*, 04021091. [[CrossRef](#)]
115. Erfani, A.; Ghanbari, A.; Massumi, A. Seismic behaviour of structures adjacent to slope by considering SSI effects in cemented soil mediums. *Int. J. Geotech. Eng.* **2021**, *15*, 2–14. [[CrossRef](#)]
116. Shamsi, M.; Shabani, M.J.; Vakili, A.H. Three-dimensional seismic nonlinear analysis of topography-structure-soi-structure interaction for buildings near slopes. *Int. J. Geomech.* **2022**, *22*, 04021295. [[CrossRef](#)]
117. Zhan, J.; Chen, G.; Jin, D. Seismic Response Characteristics of Deep Soft Site with Depth under Far-Field Ground Motion of Great Earthquake. *Adv. Mater. Res.* **2011**, *378–379*, 477–483. [[CrossRef](#)]
118. Dobry, R.; Oweis, I.; Urzua, A. Simplified procedures for estimating the fundamental period of a soil profile. *Bull. Seismol. Soc. Am.* **1976**, *66*, 1293–1321. [[CrossRef](#)]
119. Iida, M.; Iiba, M.; Kusunoki, K.; Miyamoto, Y.; Isoda, H. Relative seismic risk evaluation of various buildings based on an input wave field. *Int. J. Geomech.* **2017**, *17*, 04017068. [[CrossRef](#)]
120. Liang, J.; Jin, L.; Todorovska, M.I.; Trifunac, M.D. Soil–structure interaction for a SDOF oscillator supported by a flexible foundation embedded in a half-space: Closed-form solution for incident plane SH-waves. *Soil Dyn. Earthq. Eng.* **2016**, *90*, 287–298. [[CrossRef](#)]
121. Zhou, C.; Tian, M.; Guo, K. Seismic partitioned fragility analysis for high-rise RC chimney considering multidimensional ground motion. *Struct. Des. Tall Spec. Build.* **2018**, *28*, e1568. [[CrossRef](#)]
122. Zhang, J.; Li, M.; Han, S.; Deng, G. Estimation of seismic wave incident angle using vibration response data and stacking ensemble algorithm. *Comput. Geotech.* **2021**, *137*, 104255. [[CrossRef](#)]
123. Sebastiani, P.E.; Liberatore, L.; Lucchini, A.; Mollaioli, F. A new method to predict the critical incidence angle for buildings under near-fault motions. *Struct. Eng. Mech.* **2018**, *68*, 575–589. [[CrossRef](#)]
124. Hua, K.; Fan, L.; Che, J. Characteristics of earthquake ground motion influenced by seismic incident angle. *J. Xi'an Univ. Technol.* **2019**, *35*, 248–255. (In Chinese)
125. Zamani, N.; El Shamy, U. Discrete-element method simulations of the response of soil-foundation-structure systems to multidirectional seismic motion. *Int. J. Geomech.* **2013**, *13*, 595–610. [[CrossRef](#)]

126. Wu, C.; Yao, Q.; Yan, H.; Li, J. Nonlinear analysis of high-rise building superstructure-pile-soil mass interaction considering contact effect under severe earthquake. *Chin. J. Rock Mech. Eng.* **2011**, *30*, 3224–3233. (In Chinese)
127. Zhang, X.; Far, H. Effects of dynamic soil-structure interaction on seismic behaviour of high-rise buildings. *Bull. Earthq. Eng.* **2022**, *20*, 3443–3467. [[CrossRef](#)]
128. Zhang, X.; Far, H. Seismic response of high-rise frame-shear wall buildings under the influence of dynamic soil-structure interaction. *Int. J. Geomech.* **2023**, *23*, 04023141. [[CrossRef](#)]
129. Tabatabaiefar, S.H.R.; Fatahi, B.; Samali, B. Seismic behavior of building frames considering dynamic soil-structure interaction. *Int. J. Geomech.* **2013**, *13*, 409–420. [[CrossRef](#)]
130. Arboleda-Monsalve, L.G.; Mercado, J.A.; Terzic, V.; Mackie, K.R. Soil-structure interaction effects on seismic performance and earthquake-induced losses in tall buildings. *J. Geotech. Geoenviron. Eng.* **2020**, *146*, 04020028. [[CrossRef](#)]
131. Mercado, J.A.; Arboleda-Monsalve, L.G.; Mackie, K. Study of period lengthening effects in soil-structure interaction systems. In Proceedings of the International Foundations Congress and Equipment Expo 2021 (IFCEE 2021), Dallas, TX, USA, 10–14 May 2021; pp. 1–10. [[CrossRef](#)]
132. Stewart, J.P.; Seed, R.B.; Fenves, G.L. Seismic Soil-structure interaction in buildings. II: Empirical findings. *J. Geotech. Geoenviron. Eng.* **1999**, *125*, 38–48. [[CrossRef](#)]
133. Alexander, N.A.; Ibraim, E.; Aldaikh, H. A simple discrete model for interaction of adjacent buildings during earthquakes. *Comput. Struct.* **2013**, *124*, 1–10. [[CrossRef](#)]
134. Liang, J.; Han, B.; Todorovska, M.I.; Trifunac, M.D. 2D dynamic structure-soil-structure interaction for twin buildings in layered half-space I: Incident SH-waves. *Soil Dyn. Earthq. Eng.* **2017**, *102*, 172–194. [[CrossRef](#)]
135. Iida, M. Three-dimensional finite-element method for soil-building interaction based on an input wave field. *Int. J. Geomech.* **2013**, *13*, 430–440. [[CrossRef](#)]
136. Farahani, D.; Behnamfar, F.; Sayyadpour, H. Effect of pounding on nonlinear seismic response of torsionally coupled steel structures resting on flexible soil. *Eng. Struct.* **2019**, *195*, 243–262. [[CrossRef](#)]
137. Trombetta, N.W.; Mason, H.B.; Hutchinson, T.C.; Zupan, J.D.; Bray, J.D.; Kutter, B.L. Nonlinear soil-foundation-structure and structure-soil-structure interaction: Engineering demands. *J. Struct. Eng.* **2015**, *141*, 04014177. [[CrossRef](#)]
138. Bolisetti, C.; Whittaker, A.S. Numerical investigations of structure-soil-structure interaction in buildings. *Eng. Struct.* **2020**, *215*, 110709. [[CrossRef](#)]
139. Vicencio, F.; Alexander, N.A. Method to evaluate the dynamic structure-soil-structure interaction of 3-D buildings arrangement due to seismic excitation. *Soil Dyn. Earthq. Eng.* **2021**, *141*, 106494. [[CrossRef](#)]
140. Rayhani, M.H.T.; El Naggar, M.H. Centrifuge modeling of seismic response of layered soft clay. *Bull. Earthq. Eng.* **2007**, *5*, 571–589. [[CrossRef](#)]
141. Rayhani, M.H.T.; El Naggar, H. Physical and numerical modeling of dynamic soil-structure interaction. In Proceedings of the Geotechnical Earthquake Engineering and Soil Dynamics IV, Sacramento, CA, USA, 18–22 May 2008; pp. 1–11. [[CrossRef](#)]
142. Wang, G.; Wang, Y.; Sun, F.; Zheng, N. Experimental study on influence of foundation type on seismic response of frame structure and site soil. *World Earthq. Eng.* **2022**, *38*, 96–109. (In Chinese) [[CrossRef](#)]
143. Trombetta, N.W.; Mason, H.B.; Chen, Z.; Hutchinson, T.C.; Bray, J.D.; Kutter, B.L. Nonlinear dynamic foundation and frame structure response observed in geotechnical centrifuge experiments. *Soil Dyn. Earthq. Eng.* **2013**, *50*, 117–133. [[CrossRef](#)]
144. Trombetta, N.W.; Mason, H.B.; Hutchinson, T.C.; Zupan, J.D.; Bray, J.D.; Kutter, B.L. Nonlinear soil-foundation-structure and structure-soil-structure interaction: Centrifuge test observations. *J. Geotech. Geoenviron. Eng.* **2014**, *140*, 04013057. [[CrossRef](#)]
145. Aldaikh, H.; Alexander, N.A.; Ibraim, E.; Oddbjornsson, O. Two dimensional numerical and experimental models for the study of structure-soil-structure interaction involving three buildings. *Comput. Struct.* **2015**, *150*, 79–91. [[CrossRef](#)]
146. Li, P.; Liu, S.; Lu, Z.; Yang, J. Numerical analysis of a shaking table test on dynamic structure-soil-structure interaction under earthquake excitations. *Struct. Des. Tall Spec. Build.* **2017**, *26*, e1382. [[CrossRef](#)]
147. Fu, X.; Gao, Y.; Yang, X. Whole structure analysis of the large-span spatial structure in Jinan Olympic Stadium. *J. Build. Struct.* **2009**, *30*, 176–182. (In Chinese) [[CrossRef](#)]
148. Li, Z.; Wu, Y.; Ding, Y.; Shi, Y.; Zong, L. Amplification effect analysis of substructure on seismic response of large-span spatial hub structure. *J. Disaster Prev. Mitig. Eng.* **2021**, *41*, 823–836. (In Chinese)
149. Kato, S.; Nakazawa, S.; Saito, K. Two-mode based estimation of equivalent seismic loads and static estimation of dynamic response of reticular domes supported by ductile substructures. *J. Int. Assoc. Shell Spat. Struct.* **2006**, *47*, 35–52.
150. Masanao, N.; Yasuhito, S.; Keiji, M.; Toshiyuki, O. An efficient method for selection of vibration modes contributory to wind response on dome-like roofs. *J. Wind Eng. Ind. Aerodyn.* **1998**, *73*, 31–43. [[CrossRef](#)]
151. Feng, R.; Zhu, B.; Wang, X. A mode contribution ratio method for seismic analysis of large-span spatial structures. *Int. J. Steel Struct.* **2015**, *15*, 835–852. [[CrossRef](#)]
152. Zhao, B.; Wang, Y.; Chen, Z.; Shi, Y. State of seismic response analysis of large-span spatial structures under multi-support excitations. *Res. Steel Struct. Eng.* **2012**, *9*, 188–197. (In Chinese)
153. Bogdanoff, J.L.; Goldberg, J.E.; Schiff, A.J. The effect of ground transmission time on the response of long structures. *Bull. Seismol. Soc. Am.* **1965**, *55*, 627–640. [[CrossRef](#)]
154. Su, L.; Dong, S. Seismic analysis of two typical spatial structures under multi-support vertical excitations. *Eng. Mech.* **2007**, *24*, 85–90. (In Chinese)

155. Sun, J.; Zhang, Q. Non-stationary seismic response of long-span space cable structures under multiple support excitation. *World Earthq. Eng.* **2010**, *26*, 156–161. (In Chinese)
156. Liu, F.; Zhen, C.; Xu, Z.; Qian, J.; Zhao, J.; Ke, C.; Wang, C.; Wang, G.; Zhu, Z. Time-history analysis of terminal 3 of the Capital Airport under multi-support and multi-dimension seismic excitation. *J. Build. Struct.* **2006**, *27*, 56–63. (In Chinese) [[CrossRef](#)]
157. Shen, S.; Zhang, W.; Zhu, D.; Qian, J.; Pei, Y. Seismic response analysis of two long-span hangars under multiple support excitations. *China Civ. Eng. J.* **2008**, *41*, 17–21. (In Chinese) [[CrossRef](#)]
158. Yang, Q.; Liu, W.; Tian, Y. Response analysis of national stadium under specially variable earthquake ground motions. *China Civ. Eng. J.* **2008**, *41*, 35–41. (In Chinese) [[CrossRef](#)]
159. Jiang, Y.; Shi, Y.; Wang, Y.; Zhang, Y. Seismic response analysis of large-span gate-type tube truss structures under multi-support excitation. *J. Beijing Jiaotong Univ.* **2009**, *33*, 88–93. (In Chinese)
160. Wang, D.; Zhang, A. Anti-seismic performance experiment about the suspensdome structure of badminton gymnasium for 2008 Olympic Games. *Ind. Constr.* **2010**, *40*, 104–108. (In Chinese) [[CrossRef](#)]
161. Wang, Y.; Zhao, B.; Ding, D.; Jiang, Y.; Shi, Y.; Chen, Z. The steel structure system comparison of Hefei Xinqiao Airport Terminal based on the seismic response under multi-support excitations. *China Civ. Eng. J.* **2012**, *45*, 72–75. (In Chinese) [[CrossRef](#)]
162. *JTG 3363-2019; Specifications for Design of Foundation of Highway Bridges and Culverts*. Ministry of Transport of the People's Republic of China (MOT): Beijing, China, 2019. (In Chinese)
163. Kato, S.; Iida, M.; Minamibayashi, J. FEM analysis of elasto-plastic buckling loads of single layer latticed cylindrical roofs and estimation of the buckling loads based on the buckling stress concept. In Proceedings of the Asian Pacific Conference on Shell and Spatial Structures (APCS), Beijing, China, 21–25 May 1996; pp. 508–515.

Disclaimer/Publisher's Note: The statements, opinions and data contained in all publications are solely those of the individual author(s) and contributor(s) and not of MDPI and/or the editor(s). MDPI and/or the editor(s) disclaim responsibility for any injury to people or property resulting from any ideas, methods, instructions or products referred to in the content.